Crystal chemistry and origin of epidote-(Sr) in alkaline rocks of the teschenite association (Silesian Unit, Outer Western Carpathians, Czech Republic)

Kamil Kropáč (kamil.kropac@upol.cz)
Palacký University
Zdeněk Dolníček
National Museum
Pavel Uher
Comenius University
David Buriánek
Czech Geological Survey
Tomáš Urubek
BIC spol. s r. o. Brno: building of the Technology Innovation Transfer Chamber

Research Article

Keywords: Epidote-(Sr), Teschenite, Hydrothermal alteration, Silesian Unit, Outer Western Carpathians

Posted Date: May 10th, 2022

DOI: https://doi.org/10.21203/rs.3.rs-1621662/v1

Additional Declarations: No competing interests reported.

Version of Record: A version of this preprint was published at Mineralogy and Petrology on November 13th, 2023. See the published version at https://doi.org/10.1007/s00710-023-00847-w.

Abstract

A new occurrence of epidote-(Sr) [$CaSrAl_2Fe^{3+}(Si_2O_7)(SiO_4)(OH)$], Sr-REE-rich epidote and Sr-rich allanite-(Ce) is located in Lower Cretaceous, Sr-rich hydrothermally altered leucocratic dykes penetrating alkaline igneous rocks (teschenites) near the Nový Jičín town (the Silesian Unit, Outer Western Carpathians). The dykes contain phenocrysts of pyroxene, amphibole, biotite, fluorapatite and dominant felsic groundmass consisting mostly of alkali feldspars and zeolites (analcime, natrolite and thomsonite-Ca). Accessory minerals include Ti-rich magnetite, prehnite, chamosite, pyrite, calcite, (OH, F)-rich grossular, epidote-group minerals, HFSE-, REE-rich minerals, Sr-rich baryte and slawsonite. The Sr-rich epidote forms columnar crystals or irregular aggregates which are mostly spatially related to chamosite pseudomorphs; it contains 0.15–0.81 apfu Sr, <0.53 apfu REE; $Fe^{3+}/(Fe^{3+} + Al)$ = 0.16–0.48. The Sr^{2+} substitutes Ca^{2+} in the *A2* site by a coupled substitution involving other *A2* (REE^{3+}, Y^{3+}, Th^{4+}) or *M* (Al^{3+}, Fe^{3+}, Fe^{2+}) cations. The Sr-rich epidote crystallized from hydrothermal solutions, probably at temperatures between ~250–300 °C, during cooling of the host rock. The dykes show higher Sr contents (5680–7830 ppm) and $^{87}Sr/^{86}Sr_{i(120\ Ma)}$ ratios (~0.7046–0.7047) compared to host mesocratic teschenites (1310–1470 ppm Sr and ~0.7038–0.7045, respectively). The Sr isotopes indicate origin of most Sr from primary magmatic plagioclase in parent teschenite. Nevertheless, there participated fluids of external origin, derived from the Lower Cretaceous seawater or diagenetic waters related to associated siliciclastic sediments with $^{87}Sr/^{86}Sr_{i(120\ Ma)}$ = ~0.7073–0.7083. These more radiogenic sources contributed at least 6–21 % of the bulk Sr budget of the studied Sr-rich epidote-bearing leucocratic dykes.

Introduction

The epidote-group minerals (Armbruster et al. 2006) are locally important carriers of Sr due to a common substitution of Sr^{2+} for Ca^{2+}. In igneous and metamorphic rocks, total concentrations of Sr in epidote minerals depend on multiple factors, mainly on bulk Sr content, P-T conditions, fluid-rock interaction and presence of other potential Sr-carriers, e.g., feldspars, apatite, calcite, dolomite, aragonite, strontianite, witherite, baryte, celestine and others (Davidson 1998; Frei et al. 2004). Epidote-group minerals rich in Sr were mostly reported from HP-UHP metamorphic rocks, especially amphibolized eclogites, jadeitites and tectonized serpentinites (e.g., Brastad 1985; Mottana 1986; Harlow 1994; Nagasaki and Enami 1998), manganese deposits (Bonazzi et al. 1990; Armbruster et al. 2002; Minakawa et al. 2008; Cotterell and Tayler 2012; Tanaka and Hamane 2016), and some specific lithologies, such as metagreywacke-quartzofeldspathic schists metamorphosed under prehnite-pumpellyite to pumpellyite-actinolite facies (Grapes and Watanabe 1984), prehnite-rich rodingites derived from serpentinites (Miyajima et al. 2003), albitite dykes in serpentinized lherzolites (Monchoux et al. 2006), or hydrothermally altered peralkaline alkali-feldspar granites (Vlach 2012).

Two Sr-dominant members of the epidote-group minerals (Armbruster et al. 2006) were approved by CNMNC IMA: piemontite-(Sr) (Bonazzi et al. 1990) and epidote-(Sr) (Minakawa et al. 2008). The epidote-(Sr) [$CaSrAl_2Fe^{3+}(Si_2O_7)(SiO_4)(OH)$] was firstly reported by Minakawa et al. (2008) from hydrothermal veins in a tinzenite deposit hosted by metachert (Nagakawara deposit) and piemontite breccias (Hohnomori deposit) at the Ananai mine in Japan. Specimens from these two occurrences contain 17.1–18.0 and 10.5–16.4 wt. % SrO, respectively, and are often enriched in piemontite-(Sr) component. Cotterell and Tayler (2012) identified epidote-(Sr) and piemontite-(Sr) associated with pyrophanite in celsian from the dumps of the Fe-Mn Benallt mine (Llŷn Peninsula, United Kingdom), and Tanaka and Hamane (2016) briefly described a third occurrence of epidote-(Sr) from Shiromaru mine (low-grade Mn deposit), Japan, which forms hydrothermal veins in hematite-rich metachert.

In this work, we deal with new occurrence of epidote-(Sr) and Sr-rich epidote related to hydrothermally altered alkaline igneous rocks of the teschenite association in the Silesian Unit (Outer Western Carpathians, Czech Republic). We present data on the paragenesis, chemical composition of the Sr-rich epidote-group minerals and whole-rock Sr-isotope data and try to clarify the genesis of epidote-(Sr) and the origin of Sr for its formation.

Geological background

The investigated Sr-rich members of the epidote-group occur in leucocratic dykes penetrating mafic host rocks. Both belong to the teschenite association, which is defined as a heterogenous suite of mostly alkaline magmatic rocks geochemically equivalent to

alkaline basalts, basanites, nephelinites and picrites. The rocks of the teschenite association occur in the area between the towns of Hranice in Czech Republic and Bielsko-Biała in Poland (e.g., Pacák 1926; Smulikowski 1930; Šmíd 1978; Kudělásková 1987; Hovorka and Spišiak 1988; Włodyka and Karwowski 2004). This area belongs to the Silesian Unit of the Flysch Belt within the Outer Western Carpathians. The Silesian Unit is a part of the Krosno group of nappes, i.e., remnant of sedimentary basins developed on the margin of the European Platform and incorporated into the Carpathian accretion wedge during the Alpine orogenic event in the Cenozoic (Stráník et al. 1993; Plašienka 1997; Froitzheim et al. 2008). The Silesian Unit can be regarded as a remnant of an extensional basin formed during the Jurassic/Cretaceous rifting at the southern margin of the European Platform (Nemčok et al. 2001). Sedimentation in the Silesian Unit started in the Oxfordian-Berriasian (Eliáš 1970; Menčík et al. 1983) by shallow-water bioclastic to micritic Štramberk limestone and deep-water calcareous claystones of the Vendryně Fm. (Eliáš et al. 2003) with bodies of the Těšín limestone (Stráník et al. 1993). Typical rhythmic and cyclic flysch sedimentation started by deposition of the Hradiště Fm. during the Valanginian-Aptian (Eliáš et al. 2003). Rhythmic alternation of dark calcareous claystones and laminated sandstones is characteristic for the base of Hradiště Fm. whereas beds of sandstone and conglomerates with cobbles of the Štramberk limestone and overlying dark-gray weakly calcareous claystones dominate in the upper part.

Lithology of the Hradiště Fm. includes layers of dark organic silicites, pelocarbonate horizons and bodies of igneous rocks of the teschenite association, which form mostly hypabyssal sills, submarine extrusions, pillow lavas and volcanoclastics (Stráník et al. 1993). The ^{40}K-^{40}Ar and ^{39}Ar-^{40}Ar whole-rock dating of the teschenites reveal their Lower Cretaceous age of ~138–120 Ma (Lucińska-Anczkiewicz et al. 2002; Grabowski et al. 2003), in-situ mineral U-Pb dating gave a Lower Aptian age (~120 Ma; Szopa et al. 2014; Matýsek et al. 2018; Brunarska and Anczkiewicz 2019). The alkaline magmatism could be related with early rifting (Narebski 1990; Spišiak and Hovorka 1997; Brunarska and Anczkiewicz 2019) or with reactivation of deep faults during the Lower Cretaceous (Dostal and Owen 1998). Based on the Nd, Sr, and Hf isotopic composition and the trace element contents, the source magma was probably a product of ~2–6 % partial melting of upper mantle garnet peridotite at a depth of ~60–80 km. This magma was compositionally similar to ocean island basalts (OIB) with HIMU (high-μ; μ = ^{238}U/^{204}Pb) affinities, possibly modified by mixing with more depleted, MORB-type component (Dostal and Owen 1998; Harangi et al. 2003; Brunarska and Anczkiewicz 2019). The deposition of the Hradiště Fm. occurred above the carbonate compensation depth (Halásová et al. 2013). As a result of the Alpine orogenic event, the entire rock sequence was folded and thrusted towards NW on the Bohemian Massif (Stráník et al. 1993). Regional diagenetic thermal overprint of sediments of the Silesian Unit reached up to 170 °C (Botor et al. 2006), but local tectonic processes generated rarely vein mineralizations which formed at temperatures up to 220 °C (Dolníček et al. 2012; Urubek et al. 2014).

Strontium mineralization

Both rocks of the teschenite association and underlying carbonate sediments of the Vendryně Fm. are known for occurrence of Sr-minerals. To date, four Sr-minerals have been identified in hydrothermally altered teschenites, namely: strontianite (Dolníček et al. 2010a), slawsonite (Matýsek and Jirásek 2016; Schuchová 2016), fluorcaphite (Kropáč et al. 2017) and epidote-(Sr) (Kropáč et al. 2020 and this paper). In addition, Sr^{2+} was observed in feldspars, apatite- and epidote-group minerals, zeolites (thomsonite-Ca) and carbonates from the teschenite rocks (Spišiak and Mikuš 2008; Kynický et al. 2009; Dolníček et al. 2010a; Matýsek and Jirásek 2016; Schuchová 2016; Kropáč et al. 2017, 2020). Bulk Sr contents in the teschenites vary mostly ~600–2250 ppm (average of 23 analyses attains 1250 ppm; Dolníček et al. 2010a,b; Dostal and Owen 1998; Harangi et al. 2003; Schuchová 2016; Kropáč et al. 2017; Brunarska and Anczkiewicz 2019), but, exceptionally, Sr contents can reach up to 10320 ppm (Schuchová 2016) in the studied dykes of analcime-syenitic composition. Bulk Sr contents in picrites vary only between ~250–1290 ppm (Dostal and Owen 1998; Dolníček et al. 2010b; Brunarska and Anczkiewicz 2019) and Sr is mainly incorporated in secondary K-feldspar, carbonates and baryte (Dolníček et al. 2010b; Kropáč et al. 2015; Jirásek et al. 2017). The Sr-bearing minerals in the Vendryně Fm. are strontianite, celestine and Sr-rich baryte. The Sr- and Ba-rich hydrothermal mineralization occurs in fissures of gray-black bituminous limestone beds and concretions which are enclosed in layers of calcareous dark-gray claystones (e.g., Slavíček 1985; Jedlička 1988; Marosz and Chmiel 2007; Skýpala 2014).

Occurrence and paragenesis

The Čerťák occurrence (49°33'58"N, 17°59'54"E) is situated ca. 2 km south from the town of Nový Jičín, near a same-named water reservoir. It represents one of the best exposures of a teschenite sill, which runs in SW–NE direction between Kojetín and Bludovice villages in a total length exceeding 2 km (Fig. 1). The sill is locally over 30 m thick and compositionally heterogeneous (Matýsek and Jirásek 2016; Kropáč et al. 2020). Hydrothermally altered mesocratic fine- to coarse-grained teschenites dominates. They consist mainly of clinopyroxene and amphibole phenocrysts, biotite, apatite, analcime-feldspar groundmass, and accessory or secondary titanite, magnetite, chlorite, carbonates, and pyrite. Less common are melanocratic pyroxene-rich varieties, as well as leucocratic types (M´ = 20–35) which form up to 7 cm thick fine- to medium-grained dykes or several cm big nests randomly distributed in the mesocratic teschenite (Kropáč et al. 2020).

The mineral association of leucocratic dykes (Fig. 2) from the studied site was recently described by Matýsek and Jirásek (2016) and Kropáč et al. (2020). They consist mainly of subhedral lamellae or anhedral irregular grains of alkali feldspars (albite and K-feldspar), hyalophane, celsian (£0.21 apfu Sr) and rarely slawsonite (≤0.91 apfu Sr; Matýsek and Jirásek 2016). The alkali feldspars are surrounded or corroded by analcime and natrolite, less frequently by thomsonite-Ca with up to 0.27 apfu Sr which probably replaced primary plagioclase (Kropáč et al. 2020). Mafic components are sporadically represented by euhedral prismatic phenocrysts of clinopyroxene (diopside rimmed by hedenbergite or aegirine-augite to aegirine), long-prismatic calcic amphibole (kaersutite or ferrokaersutite with hastingsite or ferropargasite rim) and platy crystals of annite. In addition, the mineral association includes Sr-free fluorapatite (F = 0.60–1.01 apfu; own unpublished data), Ti-rich magnetite, prehnite, chlorite (chamosite), pyrite, calcite, baryte, (OH, F)-rich grossular, rare HFSE-, REE-rich accessory minerals (Zr-Nb-rich titanite, pyrochlore, zircon, REE-rich fluorapatite and vesuvianite; Kropáč et al. 2020), and epidote group minerals which are characterized in detail below.

Methods

Electron microprobe analyses were performed using Cameca SX-100 apparatus at the Masaryk University in Brno (J. Haifler and P. Gadas analysts) and the National Museum in Prague (Z. Dolníček analyst), Czech Republic. A part of BSE images were made by using electron microprobe JEOL JXA-8600 at the Palacký University in Olomouc (by J. Kapusta). The measurements were carried out on carbon-coated polished thin sections in a wavelength-dispersive mode under the following conditions: acceleration voltage 15 kV, beam current 20 nA (epidotes, titanites), 10 nA (chlorites, feldspars) or 5 nA (zeolites) and beam diameter 5 μm (chlorites, zeolites) or 1 μm (other remaining phases). The following analytical lines and standards were used: *Kα* lines: Na on albite, Al, Si and K on sanidine, P on fluorapatite, Ti on anatase, Cr on chromite, Mn on spessartine, Fe on hematite, Mg on Mg_2SiO_4, Ca on wollastonite, F on topaz and V and Cl on vanadinite; *Lα* lines: Sr on $SrSO_4$, Ba on baryte, Y on YPO_4, Zr on zircon, As on clinoclase, Sn on metallic Sn, La on $LaPO_4$, Ce on $CePO_4$, Sm on $SmPO_4$, Eu on $EuPO_4$, Gd on $GdPO_4$, Tb on $TbPO_4$, Er on $ErPO_4$, Tm on $TmPO_4$ and Yb on $YbPO_4$; *Lβ* lines: Nd on $NdPO_4$, Pr on $PrPO_4$, Ho on $HoPO_4$, Dy on $DyPO_4$ and Lu on $LuPO_4$; *Mα* lines: Pb on vanadinite and Th on cheralite; *Mβ* lines: U on metallic U. The raw counts were converted to wt. % using the automatic PAP procedure (Pouchou and Pichoir, 1985). Automatic corrections of overlaps P-Ca, F-Ce, Gd-La, Gd-Ce, and Gd-Nd were applied. The empirical formulae for epidote group minerals were normalized to the sum 8 cations and the Fe^{2+}/Fe^{3+} ratios were determined on the basis of charge balance. Determination of negative charges was performed according to recommendations of Armbruster et al. (2006): Σ (anion charge) = 2 (12 – x) + x + 1, where x = F (apfu). Analyses exceeding 3.05 apfu Si were discarded. The REE data were normalised to C1 chondrite using values given by Barrat et al. (2012). The Ce and Eu anomalies were calculated using the following equations (McLennan, 1989; Monecke et al., 2002): $Ce_{CN}/Ce^* = Ce_{CN}/\sqrt{(La_{CN}*Pr_{CN})}$; $Eu_{CN}/Eu^* = Eu_{CN}/\sqrt{(Sm_{CN}*Gd_{CN})}$. Apfu values of feldspars, chlorites, thomsonites and analcimes are based on 8, 14, 20 and 6 atoms of oxygen, respectively.

Samples for Rb, Sr, and $^{87}Sr/^{86}Sr$ determinations were powdered in an epicyclic stainless steel mill. The splits for Sr isotope determinations were decomposed using HNO_3-HCl-HF mixture. Subsequently, Sr was isolated on polypropylene columns with Sr.spec Eichrom resin. The Sr isotopic ratios were measured on a Finnigan MAT 262 thermal ionization mass spectrometer in dynamic mode using a double Re filament assembly in the isotope laboratory of the Czech Geological Survey in Prague, Czech Republic. The $^{87}Sr/^{86}Sr$ ratios were corrected for mass fractionation to $^{86}Sr/^{88}Sr = 0.1194$. External reproducibility was controlled by repeated analyses of the NBS 987 ($^{87}Sr/^{86}Sr = 0.710247 \pm 26$ (2σ), n = 25) isotopic standard. The Rb and Sr concentrations were determined in ACME analytical laboratories (Vancouver, Canada) on the same samples. The ICP-MS determination followed

decomposition of samples using $LiBO_2$ fusion and leaching of the cake in diluted 5% HNO_3. The reproducibility (better than 2 rel.%) together with precision of ICP-MS analyses of both Rb and Sr was checked by repeated analyses of the SO-18 standard. The decay constant of ^{87}Rb as high as $1.42*10^{-11}$ yr^{-1} was used for subsequent calculations (Steiger and Jäger 1977). The 'initial' $^{87}Sr/^{86}Sr_i$ ratios were calculated for the age of 120 Ma, which represents the approximate age of solidification of the host teschenite (Lucińska-Anczkiewicz et al. 2002; Grabowski et al. 2003; Szopa et al. 2014; Matýsek et al. 2018; Brunarska and Anczkiewicz 2019) and also the probable age of alteration associated with growth of Sr-rich epidote (see Discussion).

Results

Sr-rich epidote

Sr-rich epidote forms greenish to brownish columnar crystals or irregular aggregates, often with radial arrangement. They are mostly spatially related to chlorite in pseudomorphs after mafic minerals and in many cases penetrate chloritized biotite from the rim along the cleavage (Fig. 3a, b), replace apatite or clinopyroxene phenocrysts (Fig. 3c) or overgrow older hydrothermal epidote with common composition [< 0.06 apfu Sr, < 0.09 apfu REE, $Fe^{3+}/(Fe^{3+} + Al)$ = 0.18–0.19; Fig. 3d]. Some aggregates occur also in association with both secondary alkali feldspars and analcime in pseudomorphs (probably after plagioclase; Fig. 3e) and felsic groundmass (Fig. 3f). Sr-bearing epidote usually exhibits irregular patchy zoning in the BSE images. The brighter portions in BSE images contain elevated contents of Sr, Fe^{3+} and/or REE relative to Ca and Al, which concentrate in darker zones. The core is locally enriched in REE, or commonly REE-rich parts form only domains with diffuse boundaries. The SrO content varies between 2.8 and 15.9 wt. % (0.15–0.81 apfu Sr; Table 1). The contents of REE_2O_3 may reach up to 15.4 wt. % (0.53 apfu REE) with a strong dominance of La (≤0.20 apfu) and Ce (≤0.28 apfu) whereas concentrations of Y and Th are below ~ 0.03 apfu (Table 1). The calculated $Fe^{3+}/(Fe^{3+} + Fe^{2+})$ ratio ranges from 0.43 up to 1.00. The $Fe^{3+}/(Fe^{3+} + Al)$ ratio attains 0.16–0.48 whereas Al = 1.54–2.13 apfu (Table 1). Divalent Fe and Mn are regularly present in concentrations up to 0.70 and 0.10 apfu, respectively. In contrast, contents of Mg^{2+} and Ti are usually < 0.03 apfu. The ZrO_2 contents are generally low but rarely, they may reach up to 1.2 wt. % (0.06 apfu Zr). Sr-bearing epidotes are always slightly enriched in F (< 0.43 wt. %, 0.13 apfu F) and sporadically they contain up to 0.03 apfu Na^+ (Table 1). Contents of other analysed elements (P, U, Cr, Tb, Dy, Ho, Er, Tm, Yb, Lu, As, Pb, Ba, K, and Cl) are below detection limits.

The chondrite-normalized REE patterns of REE-enriched epidotes show successive decrease from La to Gd, interrupted by positive Eu anomaly (Fig. 4). The La_{CN}/Sm_{CN} ratios are rather variable and range between 6.1 and > 31.4 (Table 2). A Ce anomaly is missing or insignificant (Ce_{CN}/Ce^* = 0.84–1.26), whereas the Eu anomaly is always positive in the REE-richest epidote grains/domains (Eu_{CN}/Eu^* = 2.08 to > 4.64; Table 2).

Table 1
Representative compositions of epidote-(Sr) (Ep-Sr), Sr-REE-rich epidote (Ep) and Sr-rich allanite (Aln) from leucocratic dykes

Sa./An.	Č7/9	Č9/24	Č9/36	Č10/7	Č10/16	Č7/1	Č9/17	Č10/43	Č10/45	Č7/11
Mineral	Ep-Sr	Ep-Sr	Ep-Sr	Ep-Sr	Ep-Sr	Ep	Ep	Ep	Ep	Aln
SiO_2	34.35	34.07	34.39	32.39	33.26	32.56	34.22	31.97	32.08	31.71
TiO_2	0.13	0.12	0.12	0.06	0.18	0.17	0.29	0.20	0.33	0.10
ZrO_2	0.48	-	-	1.00	-	0.87	0.28	0.95	0.24	0.32
ThO_2	-	-	-	0.28	-	1.39	0.47	-	-	-
Al_2O_3	18.00	14.94	15.48	16.55	16.73	16.86	17.84	16.34	15.73	15.71
V_2O_3	-	na	na	0.21	0.25	-	na	0.17	0.19	-
Y_2O_3	-	-	-	0.08	-	0.23	-	0.49	0.32	0.32
La_2O_3	0.49	-	-	2.09	1.09	5.66	3.53	2.39	3.81	4.45
Ce_2O_3	0.64	0.24	-	2.70	0.99	5.52	4.11	4.21	7.32	8.09
Pr_2O_3	-	-	-	0.29	0.27	0.39	0.22	0.45	0.53	0.60
Nd_2O_3	-	-	-	0.47	0.19	0.51	0.71	1.42	1.66	1.76
Sm_2O_3	-	na	na	-	-	-	na	0.23	0.15	0.23
Eu_2O_3	-	na	na	-	-	0.09	na	0.14	0.12	0.22
Gd_2O_3	-	na	na	-	-	0.09	na	0.18	-	-
Fe_2O_3	14.36	21.84	20.80	11.38	16.05	4.87	10.63	10.02	7.77	7.41
FeO	2.27	0.21	0.58	3.39	1.00	8.05	4.84	4.70	7.05	8.85
MnO	0.41	0.14	0.11	0.25	0.07	0.90	0.24	0.25	0.29	0.51
MgO	-	-	-	-	-	-	0.08	-	-	0.08
CaO	14.81	12.78	12.68	13.59	13.25	13.08	13.77	12.75	13.22	12.07
SrO	10.01	15.35	15.93	9.41	12.65	4.44	8.38	8.54	4.67	2.80
Na_2O	-	-	-	-	0.11	-	0.06	-	-	-
F	0.19	0.05	0.12	0.28	0.18	0.43	0.29	0.28	0.38	0.35
O = F	-0.08	-0.02	-0.05	-0.12	-0.08	-0.18	-0.12	-0.12	-0.16	-0.15
Total	96.06	99.70	100.16	94.30	96.19	95.93	99.84	95.57	95.70	95.44
$^{T}Si^{4+}$	3.019	2.989	2.998	3.000	2.991	3.041	3.010	2.980	3.015	3.008
$^{T}Al^{3+}$		0.011	0.002		0.009			0.020		
Sum *T*	3.019	3.000	3.000	3.000	3.000	3.041	3.010	3.000	3.015	3.008
$^{M3}Fe^{3+}$	0.843	0.984	0.960	0.718	0.919	0.300	0.616	0.614	0.423	0.324

- Below the detection limit, na = not analyzed

Sa./An.	Č7/9	Č9/24	Č9/36	Č10/7	Č10/16	Č7/1	Č9/17	Č10/43	Č10/45	Č7/11
$^{M3}Mn^{2+}$		0.001		0.020	0.005	0.071	0.018	0.020	0.023	
$^{M3}Fe^{2+}$	0.157	0.016	0.040	0.263	0.075	0.629	0.356	0.366	0.554	0.665
$^{M3}Mg^{2+}$							0.010			0.011
$^{M2}Al^{3+}$	1.000	1.000	1.000	1.000	1.000	1.000	1.000	1.000	1.000	1.000
$^{M1}Ti^{4+}$	0.009	0.008	0.008	0.004	0.012	0.012	0.019	0.014	0.023	0.007
$^{M1}Zr^{4+}$	0.021			0.045		0.040	0.012	0.043	0.011	0.015
$^{M1}V^{3+}$				0.016	0.018			0.013	0.014	
$^{M1}Al^{3+}$	0.864	0.534	0.588	0.807	0.764	0.856	0.850	0.776	0.742	0.757
$^{M1}Fe^{3+}$	0.106	0.458	0.404	0.075	0.167	0.042	0.088	0.089	0.127	0.205
Sum *M*	3.000	3.000	3.000	2.947	2.961	2.949	2.969	2.935	2.917	2.984
$^{A2}Th^{4+}$				0.006		0.030	0.009			
$^{A2}Y^{3+}$				0.004		0.011		0.024	0.016	0.016
$^{A2}La^{3+}$	0.016			0.071	0.036	0.195	0.114	0.082	0.132	0.156
$^{A2}Ce^{3+}$	0.021	0.008		0.092	0.033	0.189	0.132	0.144	0.252	0.281
$^{A2}Pr^{3+}$				0.010	0.009	0.013	0.007	0.015	0.018	0.021
$^{A2}Nd^{3+}$				0.016	0.006	0.017	0.022	0.047	0.056	0.060
$^{A2}Sm^{3+}$								0.007	0.005	0.008
$^{A2}Eu^{3+}$						0.003		0.004	0.004	0.007
$^{A2}Gd^{3+}$						0.003		0.006		
$^{A2}Ca^{2+}$	0.435	0.211	0.195	0.349	0.296	0.309	0.308	0.274	0.331	0.306
$^{A2}Sr^{2+}$	0.510	0.781	0.805	0.505	0.660	0.240	0.427	0.462	0.254	0.154
$^{A1}Mn^{2+}$	0.031	0.010	0.008							0.041
$^{A1}Fe^{2+}$	0.010		0.002							0.038
$^{A1}Ca^{2+}$	0.959	0.990	0.989	1.000	0.981	1.000	0.990	1.000	1.000	0.921
$^{A1}Na^{+}$					0.019		0.010			
Sum *A*	1.982	2.000	2.000	2.052	2.039	2.010	2.021	2.065	2.068	2.008
Catsum	8.000	8.000	8.000	8.000	8.000	8.000	8.000	8.000	8.000	8.000
$^{O}F^{-}$	0.053	0.013	0.034	0.082	0.051	0.127	0.080	0.083	0.113	0.105
- Below the detection limit, na = not analyzed										

Table 2

REE data for the studied Sr-rich allanite (Aln), Sr-REE-rich epidote (Ep) and REE-rich epidote-(Sr) (Ep-Sr) from samples Č7 and Č10. Oxides in wt. %. The minimum possible values of La_{CN}/Sm_{CN} and Eu_{CN}/Eu^* were calculated for contents equal to detection limits

Sa./An.	Mineral	La_2O_3	Ce_2O_3	Pr_2O_3	Nd_2O_3	Sm_2O_3	Eu_2O_3	Gd_2O_3	La_{CN}/Sm_{CN}	Ce_{CN}/Ce^*	Eu_{CN}/Eu^*
Č7/11	Aln	4.45	8.09	0.60	1.76	0.23	0.22	-	12.5	1.21	> 4.64
Č7/1	Ep	5.66	5.52	0.39	0.51	-	0.09	0.09	> 31.4	0.91	> 2.66
Č7/2	Ep	3.12	4.34	0.31	0.90	-	0.11	0.12	> 17.3	1.08	> 2.82
Č7/10	Ep	3.37	6.77	0.60	1.94	0.23	0.20	-	9.4	1.16	> 4.21
Č7/12	Ep	3.72	6.61	0.56	1.68	0.25	0.16	-	9.6	1.12	> 3.23
Č10/14	Ep	3.88	5.57	0.49	1.40	0.25	0.11	-	10.0	0.98	> 2.22
Č10/15	Ep	3.19	3.75	0.33	0.85	0.20	-	-	10.3	0.89	
Č10/17	Ep	3.06	4.75	0.45	0.96	0.16	0.14	0.11	12.3	0.99	3.19
Č10/43	Ep	2.39	4.21	0.45	1.42	0.23	0.14	0.18	6.7	0.99	2.08
Č10/45	Ep	3.81	7.32	0.53	1.66	0.15	0.12	-	16.4	1.26	> 3.13
Č10/46	Ep	2.41	5.16	0.44	1.49	0.14	0.10	-	11.1	1.22	> 2.70
Č10/49	Ep	2.46	5.08	0.49	1.41	0.26	-	-	6.1	1.13	
Č10/55	Ep	3.22	6.64	0.65	1.50	0.16	0.10	-	13.0	1.12	> 2.52
Č10/56	Ep	2.15	2.99	0.30	0.65	0.16	0.13	-	8.7	0.91	> 3.28
Č10/7	Ep-Sr	2.09	2.70	0.29	0.47	-	-	-	> 11.6	0.85	

- Below the detection limit

Associated alteration minerals

The Sr-bearing epidote is often intimately associated with chlorite and titanite in pseudomorphs after clinopyroxene and biotite phenocrysts (Fig. 3a–c). Chemical composition of chlorite in pseudomorphs after pyroxene (Si = 2.85–3.04 apfu, Mn = 0.05–0.24 apfu; ≤0.04 apfu Ca, ≤ 0.03 apfu K, Fe/(Fe + Mg) = 0.80–0.97; Table 3) corresponds to chamosite (Bayliss, 1975). Chlorite from pseudomorphs after biotite usually contains elevated K (≤ 0.37 apfu) and Ti (≤ 0.05 apfu) indicating an incomplete chloritization. Anhedral titanite in the chlorite pseudomorphs after biotite contains up to 1.8 wt. % F, 8.9 wt. % Al_2O_3, 3.4 wt. % ZrO_2, and 3.2 wt. % Nb_2O_5; even more Nb-enriched titanites with up to 3.9 wt. % Nb_2O_5 form euhedral zoned crystals in the groundmass together with subhedral grains of pyrochlore (1.5–2.9 wt. % ZrO_2, ~ 1.43 apfu Nb). Rare analcime from pseudomorphs after pyroxene shows low Si content (1.78–1.85 apfu) and elevated contents of Al (~ 1.15–1.23 apfu) and Na (~ 1.13–1.21 apfu; Table 3). Exceptionally, Sr-rich thomsonite-Ca (0.05–0.27 apfu Sr) and small grains of Sr-enriched baryte, containing ~ 20.4 mol. % of celestine component, were found in the groundmass. Rare strontium feldspar slawsonite (with up to 0.74 apfu Sr and 0.15 apfu Ba), was identified only sporadically as pseudomorphs probably after plagioclase (Č7 sample). Porous aggregates of slawsonite in the pseudomorphs are associated with phyllosilicates, zeolites, and alkali feldspars, but never with Sr-bearing epidote.

Table 3
Representative compositions of some associated alteration minerals (Chl – chlorite, Anl – analcime) from epidote-bearing pseudomorphs after pyroxene (Px) and biotite (Bt)

Sa./An.	Č10/30	Č10/37	Č10/38	Č10/66	C9/40	Č10/33	Č7/41	Č7/56	Č10/72	Č9/8
Mineral	Chl	Chl	Chl	Chl	Chl	Chl	Chl	Anl	Anl	Anl
Precursor	Px	Px	Px	Px	Px	Bt	Bt	Px	Px	Px
SiO_2	23.48	26.28	24.90	25.36	24.51	25.34	27.17	45.47	49.49	47.71
TiO_2	-	0.07	-	-	-	0.96	0.97	na	na	na
Al_2O_3	16.55	17.92	16.56	16.31	16.73	16.44	16.15	26.56	26.14	26.39
MgO	0.86	3.16	4.45	4.43	2.90	1.47	1.81	-	0.12	-
CaO	0.13	0.28	0.06	0.13	0.07	0.18	0.24	0.18	-	0.06
MnO	1.32	0.73	0.56	0.58	1.33	1.49	1.34	-	-	-
FeO	43.47	37.25	40.21	40.08	42.37	41.09	38.79	-	0.25	0.06
Na_2O	0.11	-	-	-	-	-	0.37	15.51	15.62	16.44
K_2O	-	0.18	0.05	-	-	0.86	1.73	0.06	0.05	-
Total	85.92	85.87	86.79	86.89	87.91	87.83	88.57	87.78	91.67	90.66
Si^{4+}	2.853	3.035	2.907	2.951	2.870	2.963	3.109	1.781	1.847	1.810
Ti^{4+}		0.006				0.084	0.083			
Al^{3+}	2.370	2.439	2.279	2.237	2.308	2.265	2.178	1.226	1.150	1.180
Mg^{2+}	0.156	0.544	0.774	0.768	0.507	0.256	0.309		0.007	
Ca^{2+}	0.017	0.035	0.008	0.016	0.009	0.023	0.029	0.008		0.003
Mn^{2+}	0.136	0.071	0.055	0.057	0.131	0.148	0.130			
Fe^{2+}	4.417	3.597	3.926	3.901	4.150	4.018	3.712		0.008	0.002
Na^{+}	0.026						0.082	1.179	1.132	1.209
K^{+}		0.027	0.007			0.128	0.253	0.003	0.002	
Catsum	9.975	9.753	9.957	9.930	9.975	9.884	9.886	4.197	4.145	4.204
F/FM	0.97	0.87	0.84	0.84	0.89	0.94	0.92			
T (°C)	307	249	290	276	302	272	225			
T_{Si}								0.59	0.62	0.61
E (%)								2.39	0.89	-2.72

- = Below the detection limit, na = not analyzed, F/FM = Fe/(Fe + Mg), T = temperature derived from chlorite geothermometry according to Cathelineau (1988), T_{Si} = Si/(Si + Al), E = balance-error function of Passaglia (1970)

Strontium isotopes

The $^{87}Sr/^{86}Sr$ ratios were determined in related sample pairs of leucocratic dykes (Č7b and Č10b) and host mesocratic teschenite (Č7a and Č10a) from the Čerťák site. In addition, Upper Jurassic-Lower Cretaceous sediments from the Silesian Unit were also included for a comparison (Fig. 1), namely: claystone of the Hradiště Fm. (Nová Dědina site, in town of Frýdlant nad Ostravicí:

49°34'04"N, 18°21'39"E), claystone and Těšín limestone of the Vendryně Fm. (Vendryně site: 49°40'31,6"N, 18°43'07"E) and Štramberk limestone (Štramberk site: 49°35'25,8"N, 18°07'23,5"E). The present-day $^{87}Sr/^{86}Sr$ ratios in studied rocks of the teschenite association vary between 0.7040 and 0.7048 (Table 4). Leucocratic dykes show slightly higher present-day $^{87}Sr/^{86}Sr$ ratios (0.7047–0.7048) and Sr contents (568–7830 ppm) compared to host teschenites (0.7040–0.7046, 1310–1470 ppm, respectively; Table 4). In contrast, the present-day $^{87}Sr/^{86}Sr$ ratios in sedimentary rocks are considerably higher, ranging from 0.7073 (Štramberk limestone), through 0.7074 and 0.7086 (Těšín limestone and claystone of the Vendryně Fm.) to 0.7093 (claystone of the Hradiště Fm.), whereas their contents of Sr are generally much lower (196–530 ppm; Table 4).

Table 4

Rb-Sr elemental and isotope data on studied samples and calculated initial $^{87}Sr/^{86}Sr_i$ ratios for an age of 120 Ma

Sample	Sample type	Site	$^{87}Sr/^{86}Sr_m$	± 2σ	Rb (ppm)	Sr (ppm)	$^{87}Sr/^{86}Sr_i$	1000/Sr
Č7a	Host teschenite	Čerťák	0.704625	0.000008	32.4	1310	0.704503	0.76
Č7b	Leucocratic dyke	Čerťák	0.704840	0.000013	126	5680	0.704731	0.18
Č10a	Host teschenite	Čerťák	0.703957	0.000009	37.2	1470	0.703833	0.68
Č10b	Leucocratic dyke	Čerťák	0.704651	0.000010	71.7	7830	0.704606	0.13
N1	Claystone	N. Dědina	0.709280	0.000008	76.7	397	0.708326	2.52
V2	Claystone	Vendryně	0.708564	0.000006	59.4	375	0.707781	2.67
V3	Limestone	Vendryně	0.707406	0.000008	7.6	530	0.707335	1.89
Š4	Limestone	Štramberk	0.707342	0.000008	0.5	196	0.707329	5.09

Discussion

Crystal chemistry of Sr-rich epidote

A general formula for epidote-group minerals is $A_2M_3[T_2O_7][TO_4](O,F)(OH,O)$ (Armbruster et al., 2006). The monoclinic crystal structure is build by two chains of edge-sharing octahedra (parallel to the *b-axis*) that are crosslinked by isolated SiO_4 tetrahedra and Si_2O_7 groups. As a result, monoclinic members of the epidote-group have three non-equivalent octahedral sites *M1*, *M2*, and *M3* and two types of cavities *A1* and *A2* (e.g., Gieré et al. 1999; Frei et al. 2004; Franz and Liebscher 2004; Gieré and Sorensen 2004; Armbruster et al. 2006). The mineral name in the clinozoisite subgroup is derived from the dominant trivalent cation in *M3* site while the divalent cation in *A2* site determines the suffix (Armbruster et al. 2006).

In studied Sr-rich epidotes, the smaller cation site *A1* is almost fully occupied by Ca^{2+} ions with possible minor contributions of Na^{+}, Mn^{2+}, and Fe^{2+} (< 0.05 apfu). Larger and higher coordinated *A2* site is filled by Sr^{2+} and Ca^{2+} where $^{A2}Sr^{2+}/^{A2}(Sr^{2+} + Ca^{2+})$ ratio varies from 0.41 to 0.81. In addition, REE^{3+} accompanied by sporadic Y^{3+} and Th^{4+} may enter *A2* site in total concentration up to ~ 0.55 apfu. The cation site *M2* is fully occupied by Al^{3+} while in the *M1* site participate in order of quantity Al^{3+}, Fe^{3+}, Zr^{4+} and Ti^{4+}. The largest and most distorted octahedral site *M3* is dominantly occupied by Fe^{3+} (0.32–0.99 apfu). Rest of the *M3* site contains remaining octahedral cations, mainly Fe^{2+}, Mn^{2+}, Mn^{3+}, Zr^{4+}, Ti^{4+} and Al^{3+} which sporadically enters also *T* site (up to 0.04 apfu $^{T}Al^{3+}$). *O4* site contain 0.01–0.13 apfu F^{-}. The $Fe^{3+}/ (Al^{3+} + Fe^{3+})$ ratios for the *M1* and *M3* sites vary 0.00–0.46 and 0.88–1.00, respectively. Consequently, the studied minerals can be classified as epidote-(Sr) (n = 35) or Sr-rich epidote (n = 19) which exhibit, in certain cases, elevated contents of Fe^{3+} and REE^{3+}. The analysis with the highest REE^{3+} content (0.55 apfu) already corresponds to Sr-rich allanite-(Ce) (Table 1).

The relationship between *A2* cations, $^{total}Al$ and $^{M}Fe^{3+}$ illustrates Fig. 5a-h. The ^{A2}Ca vs. ^{A2}Sr diagram (Fig. 5a) shows that a simple $^{A2}Ca^{2+} \leftrightarrow {}^{A2}Sr^{2+}$ substitution is only possible in REE-free epidote-(Sr) whose analyses are located at the 1 : 1 line between the epidote and the epidote-(Sr) molecule (R^2 = -0.99). All other analyses of epidote-(Sr) and Sr-rich epidote reflects, in additional to

$^{A2}Ca^{2+} \leftrightarrow {}^{A2}Sr^{2+}$, a more complex substitution involving additional *A2* cations (REE^{3+}, Y^{3+} and Th^{4+}; Fig. 5b). Similarly, diagram ^{A2}Sr vs. $^{total}Al$ (Fig. 5c) displays good negative correlation (R^2 = -0.79) only for REE-free analyses of epidote-(Sr). On the other hand, Fig. 5d shows a clear positive correlation between $^{A2}Sr^{2+}$ and $^{M}Fe^{3+}$ (R^2 = 0.74 and 0.77) for all Sr-rich epidote minerals. The substitution mechanism for REE-free epidote-(Sr) can thus be expressed by equation: $^{A2}Ca^{2+} + {}^{M}Al^{3+} \leftrightarrow {}^{A2}Sr^{2+} + {}^{M}Fe^{3+}$, illustrating replacing of clinozoisite molecule by epidote-(Sr) one (R^2 = 0.99; Fig. 5e). However, Figs. 5e and 5f shows that the incorporation of REE^{3+}, Y^{3+}, and/or Th^{4+} into the structure is not controlled only by the Al^{3+} content. Consequently, the main substitution mechanism for REE-, Sr-rich epidote minerals can be probably expressed by a coupled heterovalent substitution: $^{A2}Ca^{2+} + {}^{A2}(REE, Y)^{3+} + {}^{M}Al^{3+} \leftrightarrow {}^{A2}Sr^{2+} + 2\ {}^{M}Fe^{3+}$ (Fig. 5g; R^2 = -0.83). For completeness, the incorporation of REE^{3+} and Y^{3+} into the *A2* site can be achieved by valence change of iron in *M3* site: $^{A2}Ca^{2+} + {}^{M3}M^{3+} \leftrightarrow {}^{A2}(REE, Y)^{3+} + {}^{M3}M^{2+}$ (Fig. 5h; R^2 = -0.78). Similarly, minor Th^{4+} may enter the *A2* site due to substitutions: $^{A2}Ca^{2+} + 2\ {}^{M3}M^{3+} \leftrightarrow {}^{A2}Th^{4+} + 2\ {}^{M3}M^{2+}$ (e.g., Bonazzi and Menchetti 1995; Gieré et al. 1999; Frei et al. 2004; Gieré and Sorensen 2004; Armbruster et al. 2006), $^{A2}Th^{4+} + {}^{M3}M^{2+} \leftrightarrow {}^{A2}(REE, Y)^{3+} + {}^{M3}M^{3+}$ or $^{A2}Th^{4+} + {}^{A2}Ca^{2+} \leftrightarrow 2\ {}^{A2}(REE, Y)^{3+}$ (Gromet and Silver 1983; Gieré et al. 1999; Wood and Ricketts 2000).

Formation conditions

The textural evidence clearly indicates an origin of epidote minerals during subsolidus hydrothermal alteration of the studied rock. In the early stage of this process, an epidote with common composition crystallized. Subsequently, the hydrothermal fluids became enriched in Sr and, to lesser extent, in REE. The assemblage of Sr-rich epidote + chlorite + titanite + analcime replacing phenocrysts of mafic minerals is typical, and offers clue for estimation of crystallization conditions. Chlorite thermometry, based on amount of tetrahedral Al (Cathelineau 1988), suggests temperatures between ~ 250 and 310°C (Table 3). Formation conditions of other associated phases were constrained in previous studies from other occurrences of teschenites in the Silesian Unit. Fluid inclusions in Al-, Nb-, Zr-poor titanites from hydrothermal veins cutting teschenites at the Tichá occurrence yielded homogenization temperatures in the interval of 390–430°C and the pressure, at which the inclusions were captured, did not exceed 1 kbar (Dolníček et al. 2010a). Analcime from the studied assemblage is characterized by distinct deficit of Si and excess of Al and Na, being typical for early analcimes, originating during initial stages of analcime crystallization (Gibb and Henderson 1978; Urubek et al. 2013). The compositionally similar early analcimes hosted by miarolitic cavities in teschenites at the Řepiště site yielded homogenization temperatures of fluid inclusions in the range of 220–300°C (Urubek et al. 2013). Taken together, the available data suggest crystallization of Sr-rich epidote at temperatures between ~ 250 and ~ 300°C and low pressures (probably < 1 kbar). Following the intrusion of teschenite bodies, the comparably high temperatures were never reached during the subsequent geological history of the Silesian Unit (cf. Botor et al. 2006; Dolníček et al. 2012; Urubek et al. 2014). This implies that hydrothermal alteration, connected with formation of the studied Sr-bearing epidote, was necessarily coincident with cooling of teschenite intrusions in the Lower Cretaceous (~ 120 Ma; Lucińska-Anczkiewicz et al. 2002; Grabowski et al. 2003; Szopa et al. 2014; Matýsek et al. 2018; Brunarska and Anczkiewicz 2019).

The highly variable La_{CN}/Sm_{CN} ratios (6.1 to > 31.4) in the studied epidote minerals indicate high degree of fractionation of REE in the parent hydrothermal fluids. This was probably related to the presence of strong REE-complexing ligands like F^-, Cl^-, OH^-, CO_3^{2-}, and/or PO_4^{3-}, which are reported to be the most effective in REE fractionation (e.g., Kwak and Abeysinghe 1987; Gieré 1990; Jiang et al. 2005; Salvi and Williams-Jones 2006; Migdisov and Williams-Jones 2014). Activity of phosphate anion is not favoured in our case due to absence of crystallization of phosphates during hydrothermal alteration. Chloride is usually a dominating species of fluid salinity and elevated F^-, OH^-, and CO_3^{2-} contents often occur in magmatic fluids exsolved during crystallization of alkaline magmas (e.g., Rubie and Gunter 1983; Marks and Markl 2017; Smith et al. 2017). Moreover, F^- undoubtedly released into co-existing fluid phase during widespread chloritization of biotite. The presence of fluorine in parent fluids is also indicated by its elevated concentrations in epidotes and associated titanites.

The strongly positive Eu anomalies in the studied epidotes (Eu_{CN}/Eu^* = 2.08 to > 4.64) indicate a high amount of Eu in the parent fluid, probably associated with coeval hydrothermal alteration of plagioclase (e.g., Jebrak et al. 1985), which is an important career of Eu in magmatic rocks (e.g., Deer et al. 2001 and references therein). In the studied rock, the textural evidence for replacing of phenocrysts of magmatic plagioclase by Sr-rich epidote was documented (Fig. 3e). Contrary to Eu^{2+}, the smaller Eu^{3+} ion has size more suitable for incorporation into the crystal structure of a hydrothermal Ca-bearing minerals (e.g., Bau 1991; Bau and Möller

1992; Lee et al. 2003). This points for a relatively high redox state of the parent fluids, confirmed also by the presence of epidote as a mineral containing high amounts of trivalent iron. It should be noted that other Fe^{3+}-rich minerals are relatively rare in products of hydrothermal alterations of teschenites in the Silesian Unit: in addition to epidote there are known occurrences of aegirine (e.g., Dolníček et al. 2010a; Buriánek and Bubík 2012) and clay mica classified as glauconite (Dolníček et al. 2010b). This is, however, expected, as hydrothermal activity occurred in a submarine environment in basic/ultrabasic igneous rocks rich in Fe^{2+}-bearing minerals and often with participation of diagenetic waters derived from surrounding organic-matter and/or pyrite bearing sediments (e.g., Dolníček et al. 2010a,b; Dolníček et al. 2012; Urubek et al. 2014; Jirásek et al. 2017). Therefore, the occurrence of Fe^{3+}-rich minerals illustrates the rare examples of activity of fluids with relatively high oxygen fugacity in teschenites, operating in case of epidote under mesothermal (~ 250–300 °C; this work) temperatures, contrary to high-temperature aegirine (~ 390–510 °C; Dolníček et al. 2010a) and low-temperature glauconite (~ 60–150 °C; Dolníček et al. 2010b).

The source of strontium

Although some authors have reported $^{87}Sr/^{86}Sr$ ratios in various rock types of the teschenite association (Dostal and Owen 1998; Harangi et al. 2003; Dolníček et al. 2010a,b; Kropáč et al. 2017; Brunarska and Anczkiewicz 2019), research focused on the source of Sr involving mineralization and associated altered host teschenites are sparse. Dolníček et al. (2010a,b) and Kropáč et al. (2017) investigated the origin of Sr in hydrothermal mineralizations associated with picrites and teschenites *s.s.* at Hončova Hůrka and Tichá occurrences, respectively. These authors suppose, based on the $^{87}Sr/^{86}Sr_{i(120\ Ma)}$ ratios, that a significant part of Sr in hydrothermal fluids must have been derived from an external source. They suggest up to three possible Sr sources, including Lower Cretaceous seawater, contemporaneous claystones of the Hradiště Fm., and underlying Upper Jurassic-Lower Cretaceous Těšín limestones of the Vendryně Fm., which contain hydrothermal mineralization with strontianite, celestite, and baryte (Skýpala 2014). The $^{87}Sr/^{86}Sr$ ratios of the Lower Cretaceous seawater range between 0.7071 and 0.7075 (Veizer et al. 1999; Fig. 6). However, only little is known about the isotopic composition of Sr in the Upper Jurassic to Lower Cretaceous sedimentary rocks of the Silesian Unit, and, likewise, the $^{87}Sr/^{86}Sr$ ratios in leucocratic dykes have not been addressed so far.

New data reveals that the highest $^{87}Sr/^{86}Sr_{i(120\ Ma)}$ ratios exhibit claystones of the Hradiště Fm. and Vendryně Fm. (0.7083 and 0.7078, respectively). Both Těšín and Štramberk limestones have similar $^{87}Sr/^{86}Sr_{i(120\ Ma)}$ ratios (0.7073), following the range reported for the Lower Cretaceous seawater (Fig. 6). In contrast, the $^{87}Sr/^{86}Sr_{i(120\ Ma)}$ ratios for most rocks of the teschenite association are considerably lower and vary only between 0.7029 and 0.7046 (Dostal and Owen 1998; Harangi et al. 2003; Dolníček et al. 2010a,b; Kropáč et al. 2017; Brunarska and Anczkiewicz 2019; Fig. 6). The studied host teschenites (Č7a and Č10a samples) have slightly lower $^{87}Sr/^{86}Sr_{i(120\ Ma)}$ ratios (0.7045 and 0.7038) than Sr-rich epidote bearing leucocratic dykes (Č7b and Č10b samples; 0.7047 and 0.7046, respectively), which indicate that their Sr isotope composition was modified during post-magmatic interaction with fluids of an external origin (i.e., diagenetic waters derived from the Upper Jurassic-Lower Cretaceous sediments of the Silesian Unit and/or Lower Cretaceous seawater). This assumption is consistent with the available geological and geochemical data. In addition, participation of externally derived fluids is well documented from previous investigations of post-magmatic vein mineralizations in the rocks of teschenite association from Silesian Unit (Dolníček et al. 2010a,b 2012; Urubek et al. 2013, 2014; Kropáč et al. 2015; Jirásek et al. 2017; Kropáč et al. 2017). Simple mass balance allows quantifying the contributions of Sr from individual sources. If we use the system claystone (Hradiště Fm.) – host teschenite, we realize that up to 6–17% of the Sr would be derived from claystones in order to explain the Sr isotopic composition of the studied leucocratic dykes. In case of the system Lower Cretaceous seawater – host teschenite, up to 8–21% of the Sr present in leucocratic dykes must originate from seawater. However, it should be noted that the calculated values are probably underestimated because hydrothermal fluids undoubtedly affected also the host teschenite itself. Nevertheless, the major source of Sr for formation of studied Sr-rich epidote and other secondary Sr-enriched minerals was in primary magmatic minerals of teschenites, namely intermediate plagioclase. Although primary plagioclase has not been preserved in the studied leucocratic dykes, its occurrence and chemical composition is known from less hydrothermally altered teschenites. For instance, relicts of primary andesine to labradorite (An_{36-52}) with 0.44–0.57 wt. % SrO occur in teschenites from the Řepiště occurrence (Kropáč et al. 2020; unpublished data of authors).

The source of REE

Although no REE isotopic data are available, it can be assumed that rocks of the teschenite association were the main source of REE. The contents of REE in rocks of the teschenite association from the Čerťák, Bludovice, and Řepiště occurrences vary in range ~ 160–340 ppm and reflect the presence of primary and secondary REE-carriers (Schuchová 2016; Kropáč et al., 2020; Safai 2020). Leucocratic dykes always display a positive Eu anomaly (up to 1.85; Kropáč et al. 2020), unlike the host teschenite, which is without Eu anomaly. The positive Eu anomaly was interpreted in terms of remobilisation of Eu from the host mesocratic teschenite and its subsequent co-precipitation with hydrothermal minerals in the leucocratic dyke (Kropáč et al. 2020). The interpretation was strengthened by the observation of primary zircon and monazite with evidence of dissolution and occurrence of hydrothermal minerals enriched in REE (Zr-, Nb-rich titanite, pyrochlore, fluorapatite, vesuvianite, and epidote; Schuchová 2016; Kropáč et al. 2017; Kropáč et al. 2020; Safai 2020; this work). In addition, the processes of REE remobilisation in rocks of teschenite associations are also illustrated by secondary bastnäsite-(Ce), synchysite-(Ce), rhabdophane-(Ce), rhabdophane-(La), cerianite-(Ce), and wakefieldite-(Ce) in microcrack fillings (Matýsek 2013).

Conclusions

The epidote-(Sr) and Sr-rich epidote in leucocratic dykes hosted by mesocratic Lower Cretaceous teschenites from the Čerťák occurrence forms together with chlorite, titanite, and analcime pseudomorphs after phenocrysts of mafic minerals or isolated crystals in the groundmass. The Sr^{2+} cation enters the structure of epidote by $^{A2}Ca^{2+} \leftrightarrow {}^{A2}Sr^{2+}$ substitution and by more complex coupled substitution involving other *A2* cations (i.e., REE^{3+}, Y^{3+} and Th^{4+}) or *M* cations (Al^{3+}, Fe^{3+} and Fe^{2+}). The Sr-rich epidote crystallized from hydrothermal solutions, probably at temperatures between ~ 250–300°C and pressure < 1 kbar, which occurred during cooling of the host teschenite sill. Leucocratic dykes have higher Sr contents and higher initial $^{87}Sr/^{86}Sr$ ratios compared to host teschenites. The Sr-isotopic composition indicates multiple sources of Sr in the studied leucocratic dyke. A major portion of Sr was originated probably from the primary plagioclase in parent teschenite. The remaining smaller part of Sr (at least 6–21%) originated from an external source, represented by either diagenetic waters derived from the neighbouring/underlying Upper Jurassic-Lower Cretaceous siliciclastic sediments of the Silesian Unit or Lower Cretaceous seawater. The research has confirmed that the occurrence of Sr-rich epidote minerals is not restricted only to HP-UHP or Mn-rich environments. Both epidote-(Sr) and Sr-REE-rich epidote can also crystallize under suitable conditions during hydrothermal alteration of Sr-enriched alkaline igneous rocks.

Declarations

Acknowledgements

This work was supported by the Palacký University Olomouc (IGA_PrF_2018_025 and IGA_PrF_2019_017) to K.K., by the Ministry of the Culture of the Czech Republic (DKRVO 2019-2023/1.II.d, 00023272) to Z.D., by the Ministry of the Environment of the Czech Republic (DKRVO/ČGS/2018-2022) to D.B. and by the EXPRO project of the Czech Science Foundation 810 (No.19-29124X) to T.U.

Author contributions

K.K. and Z.D. conceived, designed and carried out the research and wrote the main manuscript text. K.K. drafted the manuscript. P.U., D.B., and T.U. contributed to data interpretations, discussion, and revision of the manuscript.

Funding

This work was supported by the Palacký University Olomouc (IGA_PrF_2018_025 and IGA_PrF_2019_017) to K.K., by the Ministry of the Culture of the Czech Republic (DKRVO 2019-2023/1.II.d, 00023272) to Z.D., by the Ministry of the Environment of the Czech Republic (DKRVO/ČGS/2018-2022) to D.B. and by the EXPRO project of the Czech Science Foundation 810 (No.19-29124X) to T.U.

Availability of data and materials

All data presented in the text of the article are fully available without restriction from authors (K.K., Z.D., P.U., D.B., and T.U.) upon request. Code availability is not applicable.

Competing interests

The authors (K.K., Z.D., P.U., D.B., and T.U.) declare no conflicts of interest associated with this article.

References

1. Armbruster T, Gnos E, Dixon R, Gutzmer J, Hejny C, Döbelin N, Medenbach O (2002) Manganvesuvianite and tweddillite, two new Mn^{3+} minerals from the Kalahari manganese fields, South Africa. Mineral Mag 66:137–150. https://doi.org/10.1180/0026461026610018
2. Armbruster T, Bonazzi P, Akasaka M, Bermanec V, Chopin C, Gieré R, Heuss-Assbichler S, Liebscher A, Menchetti S, Pan Y, Pasero M (2006) Recommended nomenclature of epidote-group minerals. Eur J Mineral 18:551–567. https://doi.org/10.1127/0935-1221/2006/0018-0551
3. Barrat JA, Zanda B, Moynier F, Bollinger C, Liorzou C, Bayon G (2012) Geochemistry of CI chondrites: major and trace elements, and Cu and Zn isotopes. Geochim Cosmochim Acta 83:79–92. https://doi.org/10.1016/j.gca.2011.12.011
4. Bayliss P (1975) Nomenclature of the trioctahedral chlorites. Canad Mineral 13:178–185
5. Bau M (1991) Rare-earth element mobility during hydrothermal and metamorphic fluid-rock interaction and the significance on the oxidation state of europium. Chem Geol 93:219–230. https://doi.org/10.1016/0009-2541(91)90115-8
6. Bau M, Möller P (1992) Rare earth element fractionation in metamorphogenic hydrothermal calcite, magnesite and siderite. Min Petrol 45:231–246. https://doi.org/10.1007/bf01163114
7. Bonazzi P, Menchetti S (1995) Monoclinic members of the epidote group: Effect of the $Al \leftrightarrow Fe^{3+} \leftrightarrow Fe^{2+}$ substitution and the entry of REE^{3+}. Mineral Petrol 53:133–153. https://doi.org/10.1007/BF01171952
8. Bonazzi P, Menchetti S, Palenzona A (1990) Strontiopiemontite, a new member of the epidote group, from Val Graveglia, Liguria, Italy. Eur J Mineral 2:519–523. https://doi.org/10.1127/ejm/2/4/0519
9. Botor D, Dunkl I, Rauch-Włodarska M, von Eynatten H (2006) Attempt to dating of accretion in the West Carpathian Flysch Belt: apatite fission track thermochronology of tuff layers. Geolines 20:21–23
10. Brastad K (1985) Sr metasomatism, and partition of Sr between the mineral phases of a meta-eclogite from Bjørkedalen, West Norway. Tschermaks Min Petr Mitt 34:87–103
11. Brunarska I, Anczkiewicz R (2019) Geochronology and Sr–Nd–Hf isotope constraints on the petrogenesis of teschenites from the type-locality in the Outer Western Carpathians. Geol Carpath 70:222–240. https://doi.org/10.2478/geoca-2019-0013
12. Buriánek D, Bubík M (2012) Rocks of teschenite association in the surrounding of town of Valašské Meziříčí. Acta Mus Moraviae Sci geol 97(1):105–127 (in Czech)
13. Cathelineau M (1988) Cation site occupancy in chlorites and illites as a function of temperature. Clay Min 23:471–485. https://doi.org/10.1180/claymin.1988.023.4.13
14. Cháb J, Stráník Z, Eliáš M, Adamovič J, Aichler J, Babůrek J, Breiter K, Cajz V, Domečka K, Fišera M, Hanžl P, Holub V, Hradecký P, Chlupáč I, Klomínský J, Krejčí Z, Lexa J, Mašek J, Mlčoch B, Opletal M, Otava J, Pálenský P, Potfaj M, Prouza V, Roetzel R, Růžička M, Schovánek P, Slabý J, Valečka J, Žáček V (eds) (2007) Geological map of the Czech Republic 1:500 000, ČGS Praha
15. Cotterell T, Tayler R (2012) Epidote-(Sr) and Piemontite-(Sr): two minerals new to Britain from Benallt Mine, Pen Llŷn, Gwynedd, Wales. UK J Mines Minerals 33:39–42
16. Davidson J (1998) Strontium in igneous rocks, in: Geochemistry. Encyclopedia of Earth Science, edited by: Marshall, C.P., Fairbridge, R.W., Springer, Dordrecht, Netherlands. https://doi.org/10.1007/1-4020-4496-8_300
17. Deer WA, Howie RA, Zussman J (2001) Rock-forming minerals, Vol. 4A, Framework silicates: Feldspars, 2nd edn. The Geological Society, London
18. Dolníček Z, Kropáč K, Uher P, Polách M (2010a) Mineralogical and geochemical evidence for multi-stage origin of mineral veins hosted by teschenites at Tichá, Outer Western Carpathians, Czech Republic. Chem Erde-Geochem 70:267–282. https://doi.org/10.1016/j.chemer.2010.03.003
19. Dolníček Z, Urubek T, Kropáč K (2010b) Post-magmatic hydrothermal mineralization associated with Cretaceous picrite (Outer Western Carpathians, Czech Republic): interaction between host rock and externally derived fluid. Geol Carpath 61:327–339. https://doi.org/10.2478/v10096-010-0019-y

20. Dolníček Z, Kropáč K, Janíčková K, Urubek T (2012) Diagenetic source of fluids causing the hydrothermal alteration of teschenites in the Silesian Unit, Outer Western Carpathians, Czech Republic: Petroleum-bearing vein mineralization from the Stříbrník site. Mar Petrol Geol 37:27–40. https://doi.org/10.1515/geoca-2015-0003
21. Dostal J, Owen JV (1998) Cretaceous alkaline lamprophyres from northeastern Czech Republic: geochemistry and petrogenesis. Geol Rundsch 87:67–77. https://doi.org/10.1007/s005310050190
22. Eliáš M (1970) Lithology and sedimentology of the Silesian unit in the Moravskoslezské Beskydy Mts. Sborn Geol Věd Geol 18:7–99 (in Czech)
23. Eliáš M, Skupien P, Vašíček Z (2003) A proposal for the modification of the lithostratigraphical division of the lower part of the Silesian Unit in the Czech area (Outer Western Carpathians). Sbor věd Prací Vys Šk báň-Techn Univ. Ř horn-geol 49:7–15 (in Czech)
24. Franz G, Liebscher A (2004) Physical and chemical properties of the epidote minerals – An introduction. In: Liebscher A, Franz G (eds) Epidotes. Rev Mineral Geochem, vol 56. Mineralogical Society of America, Washington, pp 1–82. https://doi.org/10.2138/gsrmg.56.1.1
25. Frei D, Liebscher A, Franz G, Dulski P (2004) Trace Element Geochemistry of Epidote Minerals. Rev Mineral Geochem 56:553–605. https://doi.org/10.2138/gsrmg.56.1.553
26. Froitzheim N, Plašienka D, Schuster R (2008) Alpine tectonics of the Alps and Western Carpathians. In: McCann T (ed) Geology of Central Europe 2: Mesozoic and Cenozoic. Bonn University, Germany, pp 1141–1232. https://doi.org/10.1144/CEV2P.6
27. Gibb FGF, Henderson CMB (1978) The petrology of the Dippin sill, Isle of Arran. Scot J Geol 14:1–27. https://doi.org/10.1144/sjg14010001
28. Gieré R (1990) Hydrothermal mobility of Ti, Zr and REE: examples from the Bergell and Adamello contact aureoles (Italy). Terra Nova 2:60–67. https://doi.org/10.1111/j.1365-3121.1990.tb00037.x
29. Gieré R, Sorensen SS (2004) Allanite and other REE-rich epidote-group minerals. In: Liebscher A, Franz G (eds) Epidotes. Rev Mineral Geochem, vol 56. Mineralogical Society of America, Washington, pp 431–493. https://doi.org/10.2138/gsrmg.56.1.431
30. Gieré R, Virgo D, Popp RK (1999) Oxidation state of iron and incorporation of REE in allanite. Jour Conf Abstr 4:721. https://doi.org/10.2138/gsrmg.56.1.431
31. Grabowski J, Krzemiński L, Nescieruk P, Szydlo A, Paszkowski M, Pecskay Z, Wójtowicz A (2003) Geochronology of teschenitic intrusions in the Outer Western Carpathians of Poland–constraints from $^{40}K/^{40}Ar$ ages and biostratigraphy. Geol Carpath 54:385–393
32. Gromet LP, Silver LT (1983) Rare earth element distribution among minerals in a granodiorite and their petrogenetic implications. Geochim Cosmochim Acta 47:925–939. https://doi.org/10.1016/0016-7037(83)90158-8
33. Grapes R, Watanabe T (1984) Al-Fe^{3+} and Ca-Sr^{2+} epidotes in metagreywacke-quartzofeldspathic schist, Southern Alps, New Zealand. Am Mineral 69:490–498
34. Harangi S, Tonarini S, Vaselli O, Manetti P (2003) Geochemistry and petrogenesis of Early Cretaceous alkaline igneous rocks in Central Europe: implications for a long-lived EAR-type mantle component beneath Europe. Acta Geol Hung 46:77–94. https://doi.org/10.1556/AGeol.46.2003.1.6
35. Harlow GE (1994) Jadeitites, albitites and related rocks from the Motagua Fault Zone, Guatemala. J Metamorph Geol 12:49–68. https://doi.org/10.1111/j.1525-1314.1994.tb00003.x
36. Halásová E, Vašíček Z, Jansa L, Rehakova D, Skupien P (2012) Lower Cretaceous succession and biostratigraphy near overthrust plane of Silesian Nappe (Ostravice River Channel, Outer Western Carpathians, Czech Republic). B Geosci 87:1–25. https://doi.org/doi:10.3140/bull.geosci.1326
37. Hovorka D, Spišiak J (1988) Mesozoic Volcanism in the Western Carpathians. Veda, Bratislava, p 263. (in Slovak)
38. Jebrak M, Šmejkal V, Albert D (1985) Rare earth and isotopic geochemistry of the fluorite-barite vein deposits from the Western Rouergue district (France). Econ Geol 80:2030–2034. https://doi.org/10.2113/gsecongeo.80.7.2030
39. Jedlička J (1988) Calcium strontianite from Třinec. Čas Min geol 33:71–75 (in Czech)

40. Jiang SY, Wang RCh, Xu XS, Zhao KD (2005) Mobility of high field strength elements (HFSE) in magmatic-, metamorphic-, and submarine-hydrothermal systems. Phys Chem Earth 30:1020–1029. https://doi.org/10.1016/j.pce.2004.11.004
41. Jirásek J, Dolníček Z, Matýsek D, Urubek T (2017) Genetic aspects of barite mineralization associated with teschenite in the Silesian Unit, Outer Western Carpathians, Czech Republic. Geol Carpath 68:119–129. https://doi.org/10.1515/geoca-2017-0010
42. Kropáč K, Dolníček Z, Buriánek D, Urubek T, Mašek V (2015) Carbonate inclusions in Lower Cretaceous picrites from the Hončova hůrka Hill (Czech Republic, Outer Western Carpathians): Evidence for primary magmatic carbonates? Int J Earth Sci 104:1299–1315. https://doi.org/10.1007/s00531-015-1152-8
43. Kropáč K, Dolníček Z, Uher P, Buriánek D, Safai A, Urubek T (2020) Zirconian–niobian titanite and associated Zr-, Nb-, REE-rich accessory minerals: Products of hydrothermal overprint of leucocratic teschenites (Silesian Unit, Outer Western Carpathians, Czech Republic). Geol Carpath 71:343–360. https://doi.org/10.31577/GeolCarp.71.4.4
44. Kropáč K, Dolníček Z, Uher P, Urubek T (2017) Fluorcaphite from hydrothermally altered teschenite at Tichá, Outer Western Carpathians, Czech Republic: compositional variations and origin. Mineral Mag 81:1485–1501. https://doi.org/10.1180/minmag.2017.081.016
45. Kudělásková J (1987) Petrology and geochemistry of selected rock types of teschenite association, Outer Western Carpathians. Geol Carpath 38:545–573
46. Kynický J, Xu Ch, Bajer A, Samec P, Kynická A (2009) New exploration of teschenite clan rocks: Sr and REE-rich fluorapatites. Geol Výzk Mor Slez 16:66–69 (in Czech)
47. Kwak TAP, Abeysinghe PB (1987) Rare earth and uranium minerals present as daughter crystals in fluid inclusions, Mary Kathleen U-REE skarn, Queensland, Australia. Mineral Mag 51:665–670. https://doi.org/10.1180/minmag.1987.051.363.05
48. Lee SG, Lee DH, Kim Y, Chae BG, Kim WY, Woo NCh (2003) Rare earth elements as indicators of groundwater environment changes in a fractured rock system: evidence from fracture – filling calcite. Appl Geoch 18:135–143. https://doi.org/10.1016/S0883-2927(02)00071-9
49. Lucińska-Anczkiewicz A, Villa IM, Anczkiewicz R, Ślaczka A (2002) $^{40}Ar/^{39}Ar$ dating of alkaline lamprophyres from the Polish Western Carpathians. Geol Carpath 53:45–52
50. Marosz K, Chmiel E (2007) New occurrences of strontium mineralization in Třinec area. Minerál 15:198–202
51. Marks AWM, Markl G (2017) A global review on agpaitic rocks. Earth-Sci Rev 173:229–258
52. Matýsek D (2013) Evidence of rare earth elements (REE) mobilization in teschenites of the Beskydy Mts. region. Acta Mus Moraviae Sci geol 2:101–113 (in Czech)
53. Matýsek D, Jirásek J (2016) Occurrences of slawsonite in rocks of the teschenite association in the Podbeskydí Piedmont area (Czech Republic) and their petrological significance. Can Mineral 54:1129–1146. https://doi.org/10.3749/canmin.1500101
54. Matýsek D, Jirásek K, Skupien P, Thomson SN (2018) The Žermanice sill: new insights into the mineralogy, petrology, age, and origin of the teschenite association rocks in the Western Carpathians, Czech Republic. Int J Earth Sci 107:2553–2574. https://doi.org/10.1007/s00531-018-1614-x
55. McLennan SM (1989) Rare earth elements in sedimentary rocks: influence of provenance and sedimentary processes. Rev Mineral 21:169–200. https://doi.org/10.1515/9781501509032-010
56. Menčík E, Adamová M, Dvořák J, Dudek A, Jetel J, Jurková A, Hanzlíková E, Houša V, Peslová H, Rybářová L, Šmíd B, Šebesta J, Tyráček J, Vašíček Z (1983) Geology of the Moravskoslezské Beskydy Mts. and the Sub-Beskidian Highland. Ústř Úst geol Nakl Čs akad Věd, Praha, p 307. (in Czech)
57. Minakawa T, Fukushima H, Nishio-Hamane D, Miura H (2008) Epidote-(Sr), $CaSrAl_2Fe^{3+}(Si_2O_7)(SiO_4)(OH)$, a new mineral from the Ananai mine, Kochi Prefecture, Japan. J Mineral Petrol Sci 103:400–406. https://doi.org/10.2465/jmps.071220
58. Miyajima H, Matsubara S, Miyawaki R, Hirokawa K (2003) Niigataite, $CaSrAl_3(Si_2O_7)(SiO_4)O(OH)$: Sr-analogue of clinozoisite, a new member of the epidote group from the Itoigawa-Ohmi district, Niigata Prefecture, central Japan. J Mineral Petrol Sci 98:118–129. https://doi.org/10.2465/jmps.98.118
59. Migdisov A, Williams-Jones AE (2014) Hydrothermal transport and deposition of the rare earth elements by fluorine-bearing aqueous liquids. Mineral Deposita 49:987–997. https://doi.org/10.1007/s00126-014-0554-z

60. Monchoux P, Fontan F, De Parseval P, Martin RF, Wang RC (2006) Igneous albitite dikes in orogenic lherzolithes, Western Pyrénées, France: A possible source for corundum and alkali feldspar xenocrysts in basaltic terranes, I. Mineralogical Associations. Can Mineral 44:817–842. https://doi.org/10.2113/gscanmin.44.4.817
61. Monecke T, Kempe U, Monecke J, Sala M, Wolf D (2002) Tetrad effect in rare earth element distribution patterns: a method of quantification with application to rock and mineral samples from granite-related rare metal deposits. Geochim Cosmochim Acta 66:1185–1196. https://doi.org/10.1016/S0016-7037(01)00849-3
62. Mottana A (1986) Blueschist-facies metamorphism of manganiferous cherts: a review of the alpine occurrences. In: Evans BW, Brown EH (eds) Blueschists and Eclogites, vol 164. Mem Geol Soc Am, pp 267–299. https://doi.org/10.1130/MEM164-p267
63. Nagasaki A, Enami M (1998) Sr-bearing zoisite and epidote in ultra-high pressure (UHP) metamorphic rocks from the Su-Lu province, eastern China: An important Sr reservoir under UHP conditions. Am Mineral 83:240–247. https://doi.org/10.2138/am-1998-3-407
64. Narebski W (1990) Early rift stage in the evolution of western part of the Carpathians: geochemical evidence from limburgite and teschenite rock series. Geol Carpath 41:521–528
65. Nemčok M, Nemčok J, Wojtaszek M, Ludhova L, Oszczypko N, Sercombe WJ, Cieszkowski M, Paul Z, Coward MP, Ślaczka A (2001) Reconstruction of Cretaceous rifts incorporated in the Outer West Carpathian wedge by balancing. Mar Petrol Geol 18:39–64. https://doi.org/10.1016/S0264-8172(00)00045-3
66. Pacák O (1926) Volcanic rocks at the northern foothill of the Moravské Beskydy Mts. Česká Akad Věd a Umění, Praha, p 232. (in Czech)
67. Passaglia E (1970) The crystal chemistry of chabazites. Am Mineral 55:1278–1301
68. Plašienka D, Grecula P, Putiš M, Kováč M, Hovorka D (1997) Evolution and structure of the Western Carpathians: an overview. In: Grecula P, Hovorka D, Putiš M (eds) Geological Evolution of the Western Carpathians. Miner Slovaca – Monograph, Bratislava, Slovakia, pp 1–24
69. Pouchou J, Pichoir F (1985) "PAP" procedure for improved quantitative microanalysis. Microbeam Anal 20:104–105
70. Rubie DC, Gunter WD (1983) The role of speciation in alkaline igneous fluids during fenite metasomatism. Contr Mineral Petrol 82:165–175
71. Safai A (2020) Distribution of selected high-field-strength elements in the rock of the teschenite association. MSc Thesis, Palacký University Olomouc (in Czech)
72. Salvi S, Williams-Jones AE (2006) Alteration, HFSE mineralization and hydrocarbon formation in peralkaline igneous systems: Insights from the Strange Lake Pluton, Canada. Lithos 91:19–34. https://doi.org/10.1016/j.lithos.2006.03.040
73. Schuchová K (2016) Petrographic Variability of Teschenites from the Site Bludovice near Nový Jičín. MSc Thesis, Palacký University Olomouc (in Czech)
74. Skýpala J (2014) Strontium Mineralization of the Těšín Limestone (Silesian Unit, Outer Western Carpathians). BSc Thesis, Palacký University Olomouc (in Czech)
75. Slavíček P (1985) New occurrence of strontianite in Těšín limestones near Třinec. Čas Min geol 30:213–214 (in Czech)
76. Smith DJ, Naden J, Jenkin GRT, Keith M (2017) Hydrothermal alteration and fluid pH in alkaline-hosted epithermal systems. Ore Geol Rev 89:772–779
77. Smulikowski K (1930) Les roches éruptives de la zone subbeskidique en Silésie et Moravie. Kosmos 54:749–850 (in French)
78. Spišiak J, Hovorka D (1997) Petrology of the Western Carpathians Cretaceous primitive alkaline volcanics. Geol Carpath 48:113–121 (in Slovak)
79. Spišiak J, Mikuš T (2008) Ba- and Sr-rich phases in Cretaceous alkaline volcanites of the Outer Western Carpathians. Geochémia 2008 proceedings, ŠGÚDŠ Bratislava 135–137 (in Slovak)
80. Steiger RH, Jäger E (1977) Subcommission on geochronology: convention on the use of decay constant in geo- and cosmochronology. Earth Planet Sci Lett 36:359–362. https://doi.org/10.1016/0012-821X(77)90060-7
81. Stráník Z, Menčík E, Eliáš M, Adámek J (1993) Flysch belt of the West Carpathians, autochthonous Mesozoic and Paleogene in Moravia and Silesia. In: Přichystal A, Obstová V, Suk M (eds) Geology of Moravia and Silesia. Mor zem muz. PřF MU, Brno, pp 107–122. (in Czech)

82. Szopa K, Włodyka R, Chew D (2014) LA-ICP-MS U-Pb apatite dating of Lower Cretaceous rocks from teschenite-picrite association in the Silesian Unit (southern Poland). Geol Carpath 65:273–284. https://doi.org/10.2478/geoca-2014-0018
83. Šmíd B (1978) The Investigation of Igneous Rocks of the Teschenite Association. MS, Central Geological Survey, Prague, p 153. (in Czech)
84. Tanaka T, Hamane D (2016) Epidote-(Sr) from Shiromaru mine, Tokyo prefecture, Japan. (conference presentation R1-P14)
85. Urubek T, Dolníček Z, Kropáč K, Lehotský T (2013) Fluid inclusions and chemical composition of analcimes from Řepiště site (Outer Western Carpathians). Geol Výzk Mor Slez 20:107–111 (in Czech)
86. Urubek T, Dolníček Z, Kropáč K (2014) Genesis of syntectonic hydrothermal veins in the igneous rock of teschenite association (Outer Western Carpathians, Czech Republic): growth mechanism and origin of fluids. Geol Carpath 65(6):419–431. https://doi.org/10.1515/geoca-2015-0003
87. Veizer J, Ala D, Azmy K, Bruckschen P, Bruhl D, Bruhn F, Carden GAF, Diener A, Ebneth S, Godderis Y, Jasper T, Korte Ch, Pawellek F, Podlaha OG, Strauss H (1999) $^{87}Sr/^{86}Sr$, $\delta^{13}C$ and $\delta^{18}O$ evolution of Phanerozoic seawater. Chem Geol 161:59–88. https://doi.org/10.1016/S0009-2541(99)00081-9
88. Vlach SRF (2012) Micro-structural and compositional variations of hydrothermal epidote-group minerals from a peralkaline granite, Corupá Pluton, Graciosa Province, South Brazil, and their petrological implications. An Acad Bras Ciênc 84(2):405–423. https://doi.org/10.1590/S0001-37652012005000024
89. Włodyka R, Karwowski Ł (2004) The alkaline magmatism from the Polish Western Carpathians. Pol Tow Miner, Pr Spec 24:23–31
90. Wood SA, Ricketts A (2000) Allanite-(Ce) from Eocene Casto Granite, Idaho: Response to hydrothermal alteration. Can Mineral 38:81–100. https://doi.org/10.2113/gscanmin.38.1.81

Figures

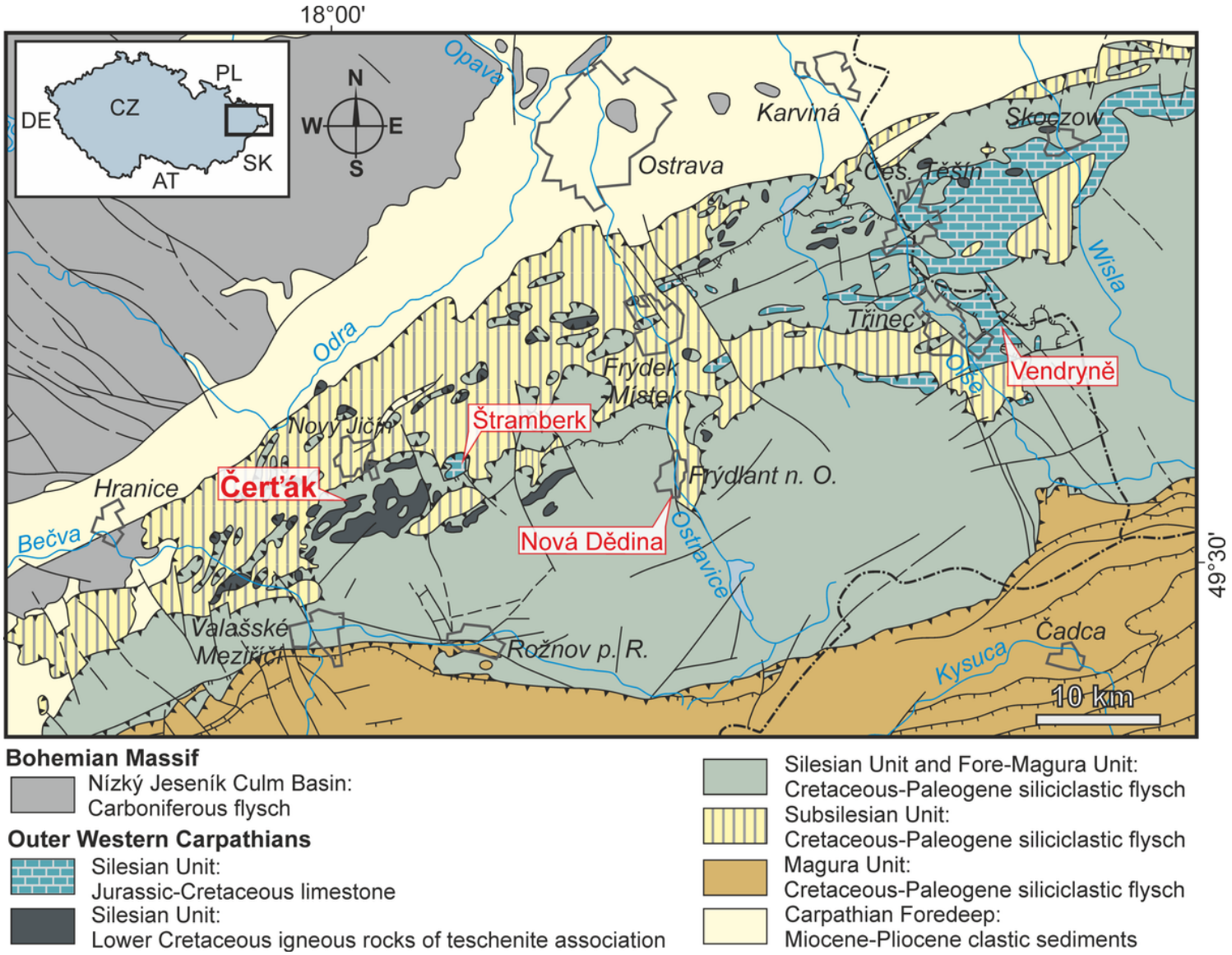

Figure 1

Geological position of the Čerťák teschenite sill and position of localities where Upper Jurassic-Lower Cretaceous sediments were sampled (Štramberk, Vendryně and Nová Dědina) (modified according to Cháb et al. 2007)

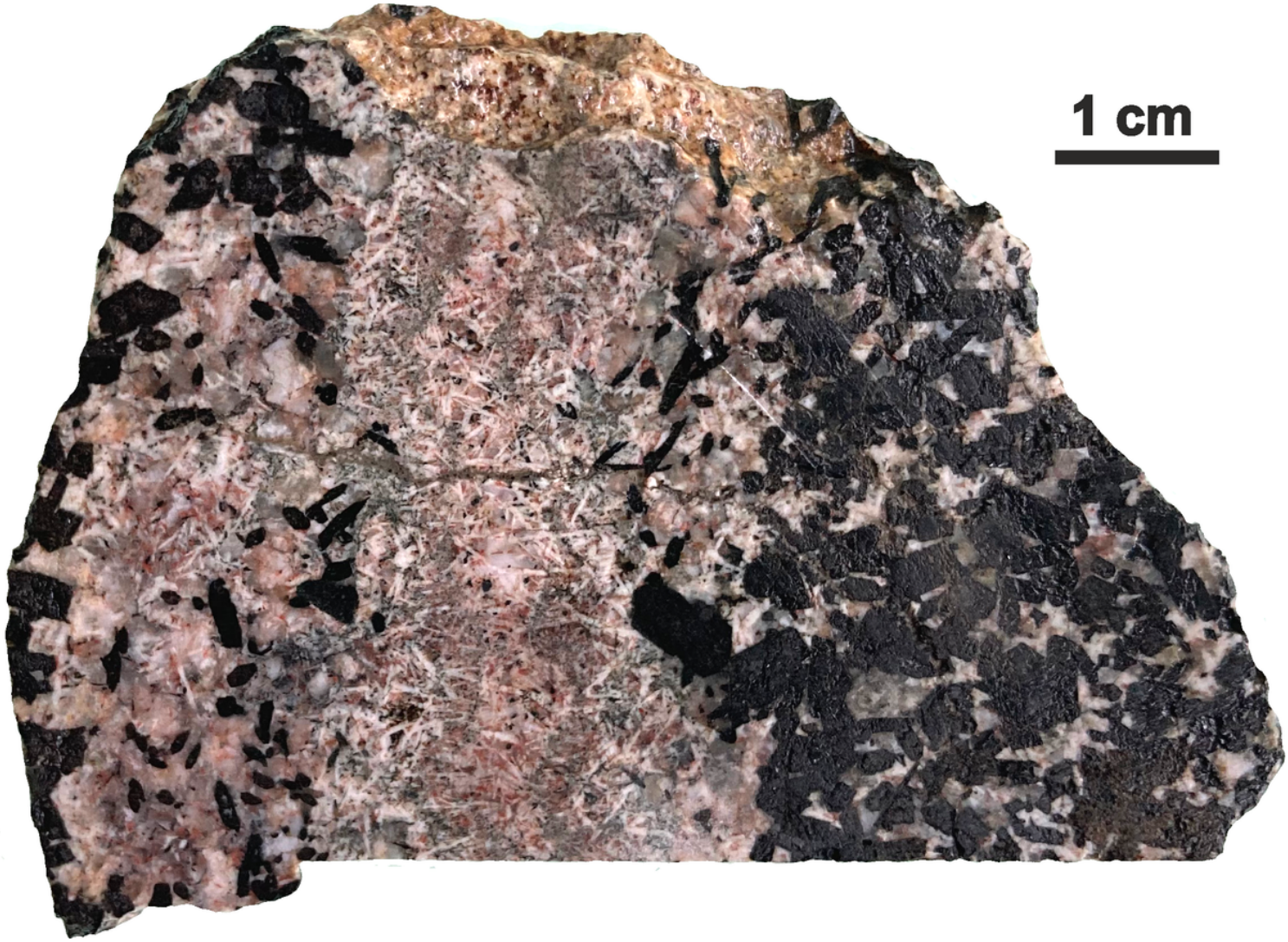

Figure 2

Macroscopic appearance of leucocratic dyke and host mesocratic teschenite (sample Č7)

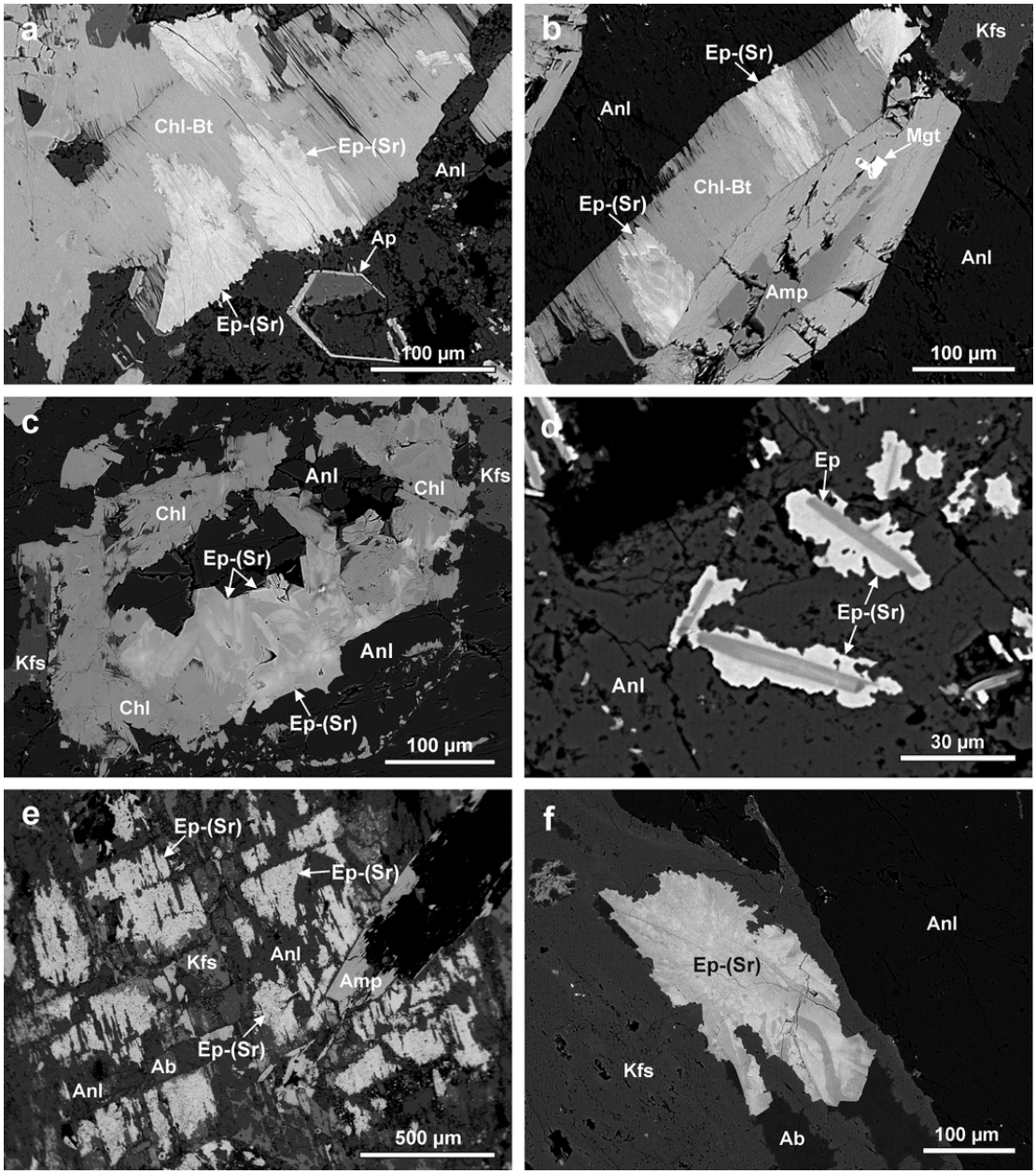

Figure 3

Morphology and association of studied epidote-(Sr) from sample Č9 in BSE images: a, b) irregular aggregates of epidote-(Sr) growing along the cleavage of chloritized biotite; c) irregular patchy zoning of epidote-(Sr) in chlorite pseudomorph after clinopyroxene; d) the epidote-(Sr) overgrown on older hydrothermal epidote columns with common composition; e) aggregates of epidote-(Sr) in association with secondary alkali feldspars and analcime in pseudomorph after plagioclase; f) irregular aggregates of epidote-(Sr) with radial arrangement associated with secondary alkali feldspars and analcime. Abbreviations: Ab – albite, Amp – amphibole, Anl – analcime, Ap – apatite, Bt – biotite, Chl – chlorite, Ep – epidote, Ep-(Sr) – epidote-(Sr), Kfs – K-feldspar

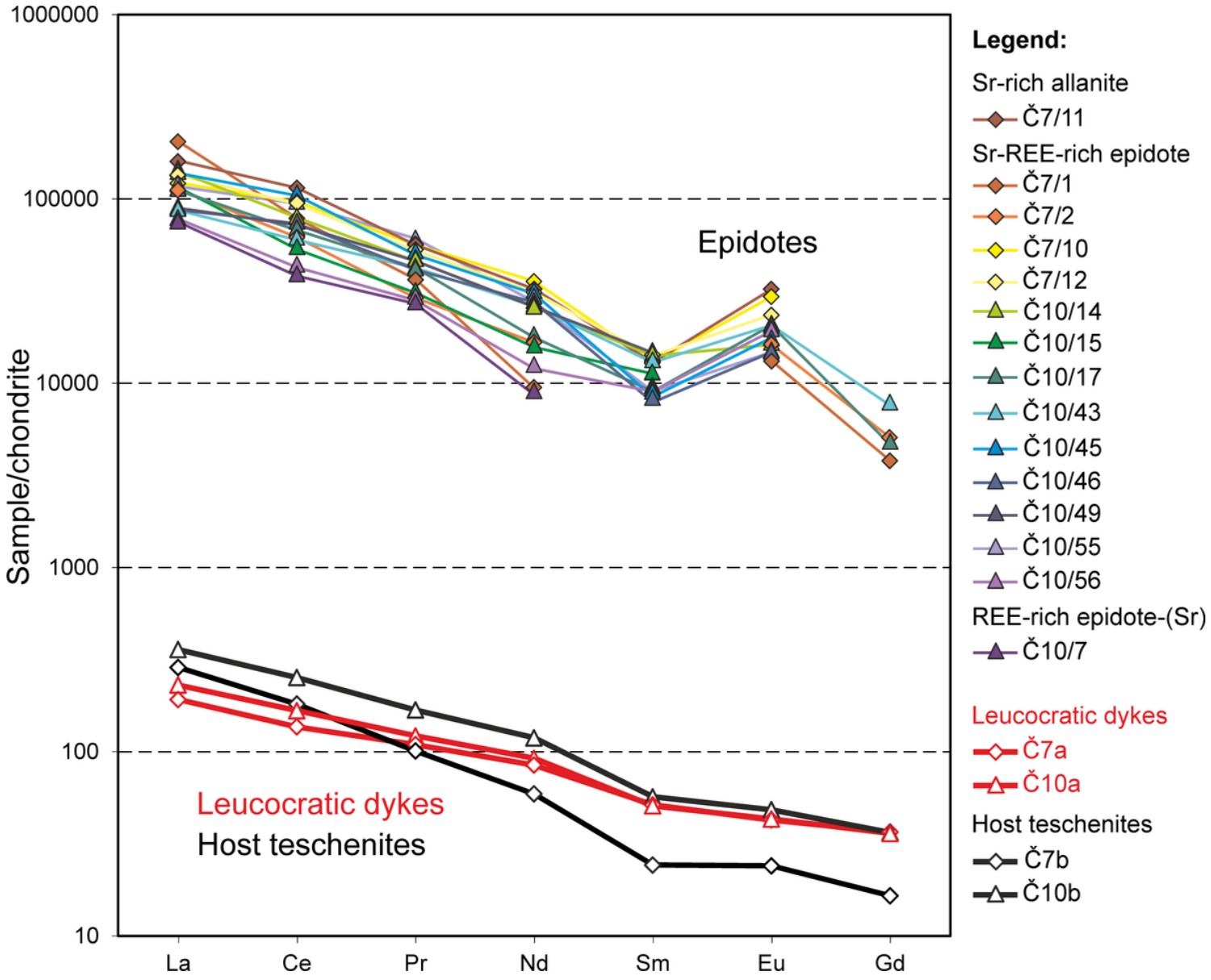

Figure 4

Selected representative chondrite-normalised patterns of the studied Sr+REE-richer epidote minerals from samples Č7 and Č10. The whole-rock data from the studied samples are from Safai (2020)

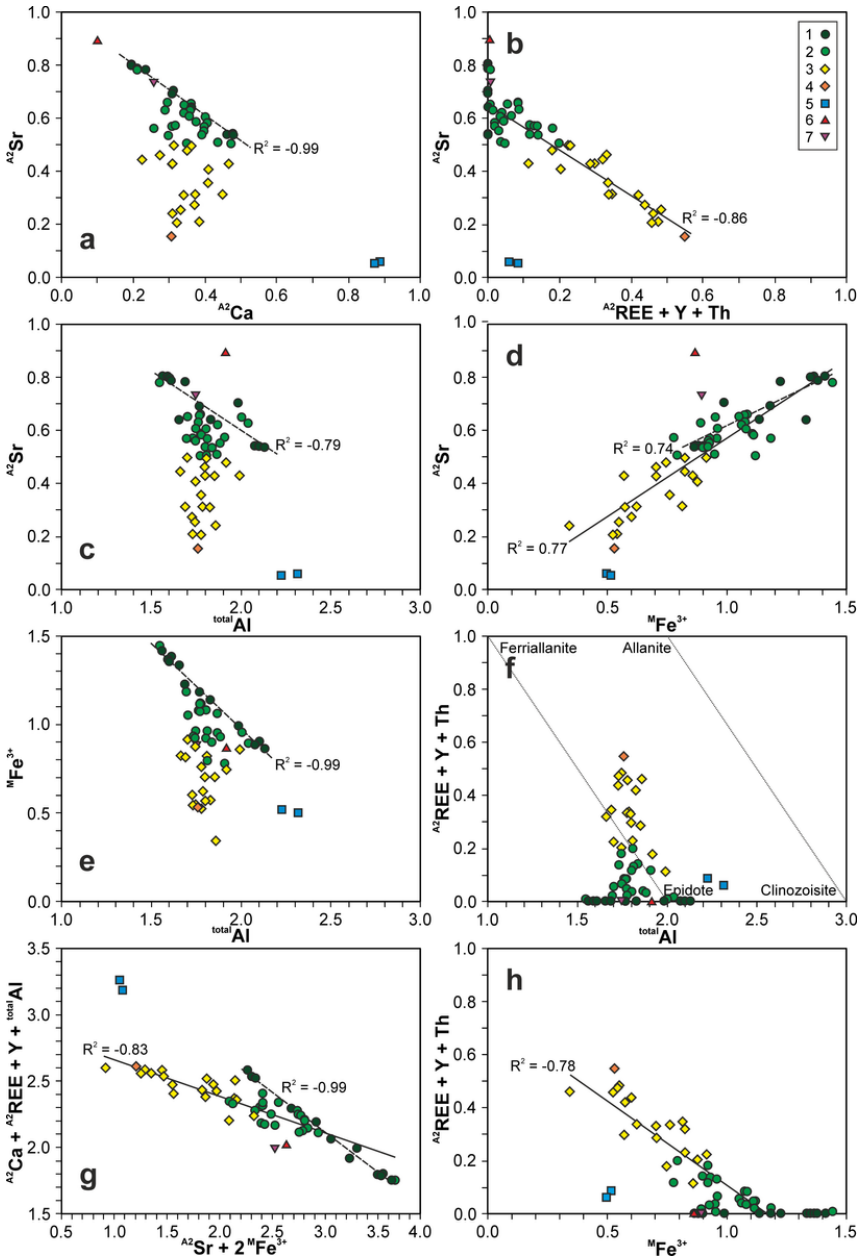

Figure 5

Substitution diagrams showing the relationship among contents (apfu) of Sr, Ca, ^{total}Al, ^{M}Fe^{3+}, REE, Y and Th. Legend: 1, 2 – epidote-(Sr) from Čerťák: (1) REE + Y + Th = 0.00 apfu, (2) ≥ 0.01 apfu; 3 – Sr-rich epidote from Čerťák; 4 – Sr-rich allanite-(Ce) from Čerťák; 5 – epidote from Čerťák; 6, 7 – composition of epidote-(Sr) from Nagakawara and Hohnomori, respectively (Minakawa et al. 2008). R^2 values were calculated separately for REE(Y, Th)-free (dashed line) and REE(Y, Th)-rich (full line) analyses of Sr-rich epidote minerals from the Čerťák site (i.e., no. 1–4; zero values are not included)

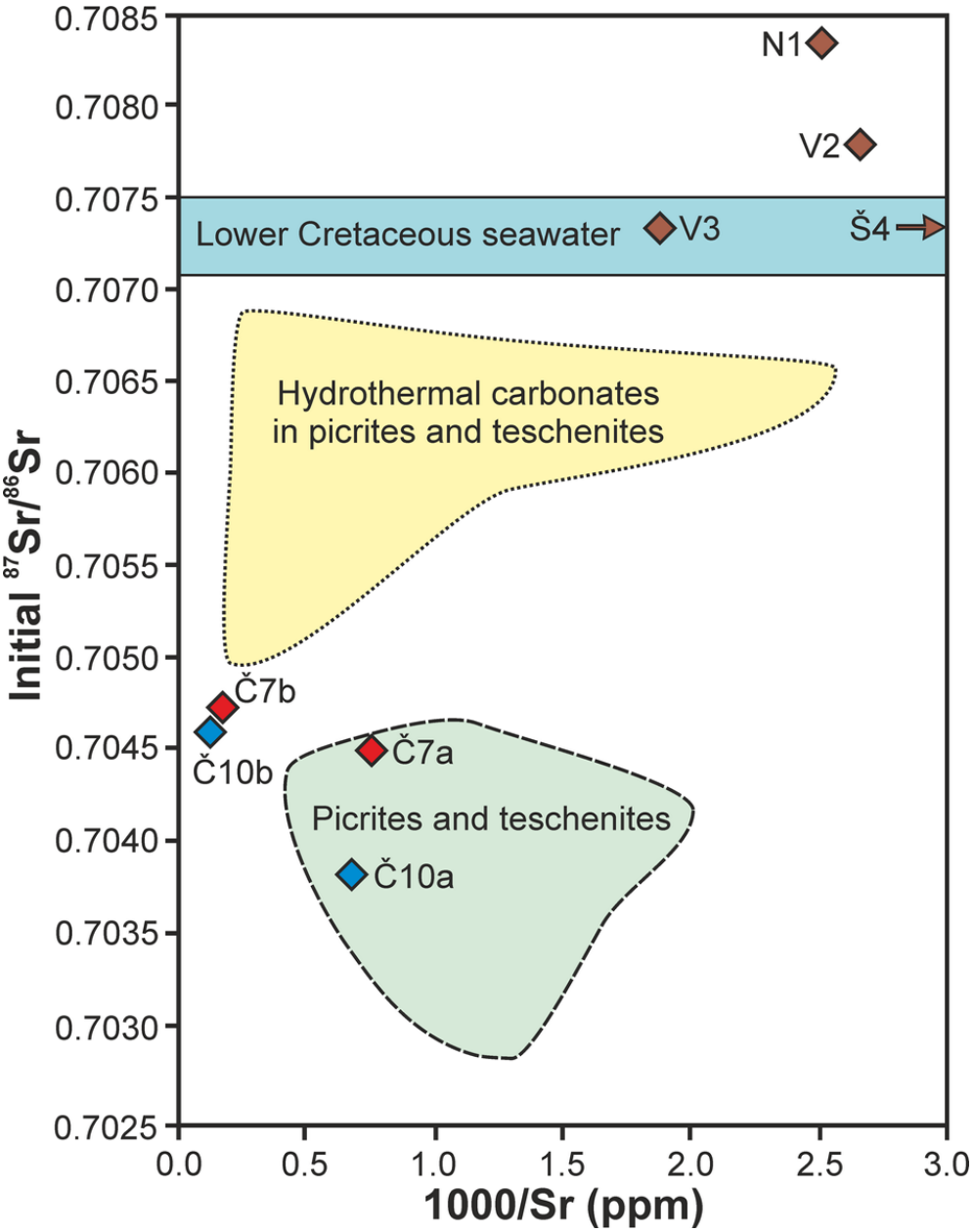

Figure 6

$^{87}Sr/^{86}Sr_i$ vs. 1000/Sr plot for samples of leucocratic dykes (Č7b and Č10b) and host teschenite (Č7a and Č10a) from the Čerťák site and for sedimentary rocks of the Silesian Unit (N1, V2, V3, and Š4). $^{87}Sr/^{86}Sr_i$ of the Štramberk limestone (Š4) is marked only by arrow due to its low Sr content (1000/Sr = 5.09). The field for picrites and teschenites shows representative analyses of rocks of the teschenite association from various sites in the Silesian Unit (Dostal and Owen 1998; Harangi et al. 2003; Dolníček et al. 2010a,b; Kropáč et al. 2017; Brunarska and Anczkiewicz 2019). The field for hydrothermal carbonates in picrites and teschenites is according to Dolníček et al. (2010a,b) and Kropáč et al. (2017). The range of $^{87}Sr/^{86}Sr$ ratios for the Lower Cretaceous seawater is according to Veizer et al. (1999)